EASTLAND PORT MAINTENANCE DREDGING AND DISPOSAL PROJECT

Dredging Plume Modelling - Maintenance Dredging

Report prepared for Eastland Port

December 2019

MetOcean SOLUTIONS

MetOcean Solutions: Report P0331

December 2019

Report status

Version	Date	Status	Approved by
RevA	02/04/2018	Draft for internal review	Weppe
RevB	12/12/2019	Updated draft	Weppe
RevC	13/12/2019	Draft for Client review	Berthot

TABLE OF CONTENTS

LIST OF FIGURES

LIST OF TABLES

1. INTRODUCTION

Eastland Port Ltd, Gisborne are required to renew their maintenance dredging and disposal consents (Figure 1-1). The existing permits for channel maintenance dredging and disposal at both the offshore and inshore sites (issued by the Environment Court, August 2000) elapsed August 2015, while consents to dredge alongside berths 4, 5 and 6 to 7 m chart datum and disposal of the sediment at the offshore disposal ground were gained in 2013 and will expire on 30th June 2018.

Currently, dredged sediment is disposed at an offshore disposal site (Figure 1-1) situated in approximately 18 – 20 m water depth, with an average annual maintenance disposal rate of approximately 100,000 m^3 (based on values between 2009 and 2015).

Maintenance dredging is expected to occur using the “Pukunui” Trailing Suction Hopper Dredge (TSHD) although, if there are significant inflows of sediment due to large storm events, a higher productivity (i.e. larger TSHD) may be used to ensure the required port and channel depths are maintained.

MetOcean Solutions (MOS) has been contracted to provide coastal oceanographic expertise to investigate both physical and morphological effects and associated sediment transport patterns resulting from the dredging and disposal of maintenance dredging material at the proposed disposal site.

A previous report (MetOcean Solutions, 2017) presented the implementation and validation of the Poverty Bay hydrodynamic modelling at regional and local scales. Sediment plume and deposition patterns associated with the sediment disposal operations were characterised in (MetOcean Solutions, 2018) report.

The present report focuses on the characterisation of the sediment plume patterns expected during the dredging operations. Dredging operations were simulated using particle-tracking modelling over two different 1-year periods within contrasting historical contexts, namely El Niño/La Niña episodes. The applied methodology is provided in Section 2, including a description of the particle-tracking model, sediment distribution and dredging scenarios. Simulations results are presented and interpreted in Section 3 and a brief summary concludes the report in Section 4. All references cited within the report a listed in Section 5.

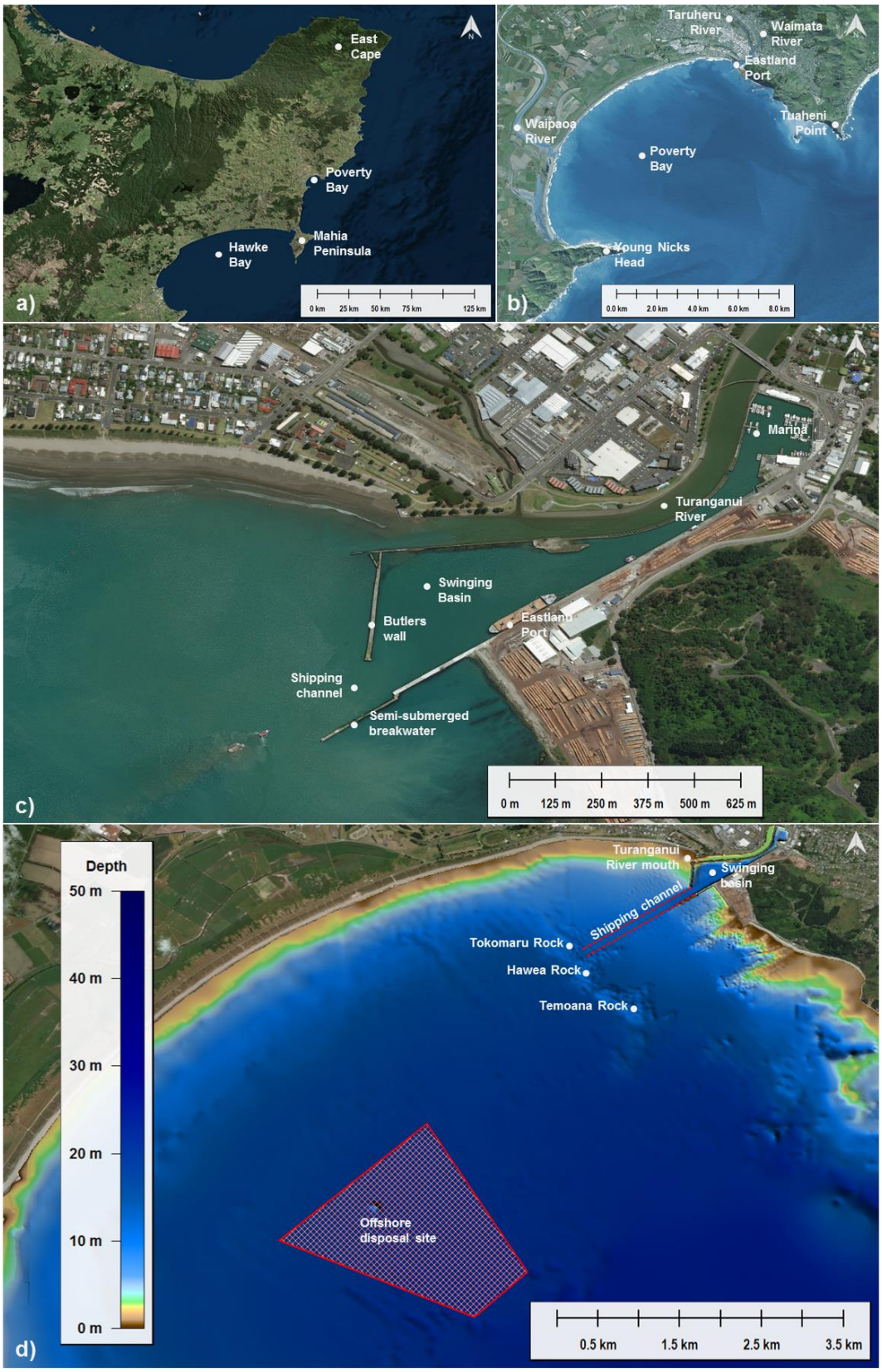

Figure 1-1 Maps showing the location of Poverty Bay (a and b), and Eastland Port (c) with the locations used in the present study. Both offshore disposal and shipping channel are indicated on top of the bathymetry in (d).

2. METHODS

2.1. Approach

An actual release of sediment in the oceanic environment is a process that is finite in time (i.e. occurring at a specific time, over a finite period) and inherently non-deterministic (i.e. controlled by a range of random and unpredictable variables such as currents and turbulences). Since future ocean conditions, and exact timing modes of the dredging works are unknown, it is not possible to predict the actual outcomes of a release before the event occurs. However, the probability of future oceanic conditions can be assessed from the historical conditions, thereby allowing "probabilistic" estimations of the geographical dispersion of the suspended sediment plume patterns.

In the present study, dredging operations were simulated during two 1-year periods with contrasting ambient forcing regimes of La Niña and El Niño (June 1998-June 1999, and June 2002-June 2003, respectively). A range of dredging locations (Figure 2-1) and operating modes were considered to assess effects on the generated plumes. These long-term simulations allow capturing the variability of current forcing expected on an annual timescale and provide a robust basis to derive probabilistic dispersion patterns and compare outcomes.

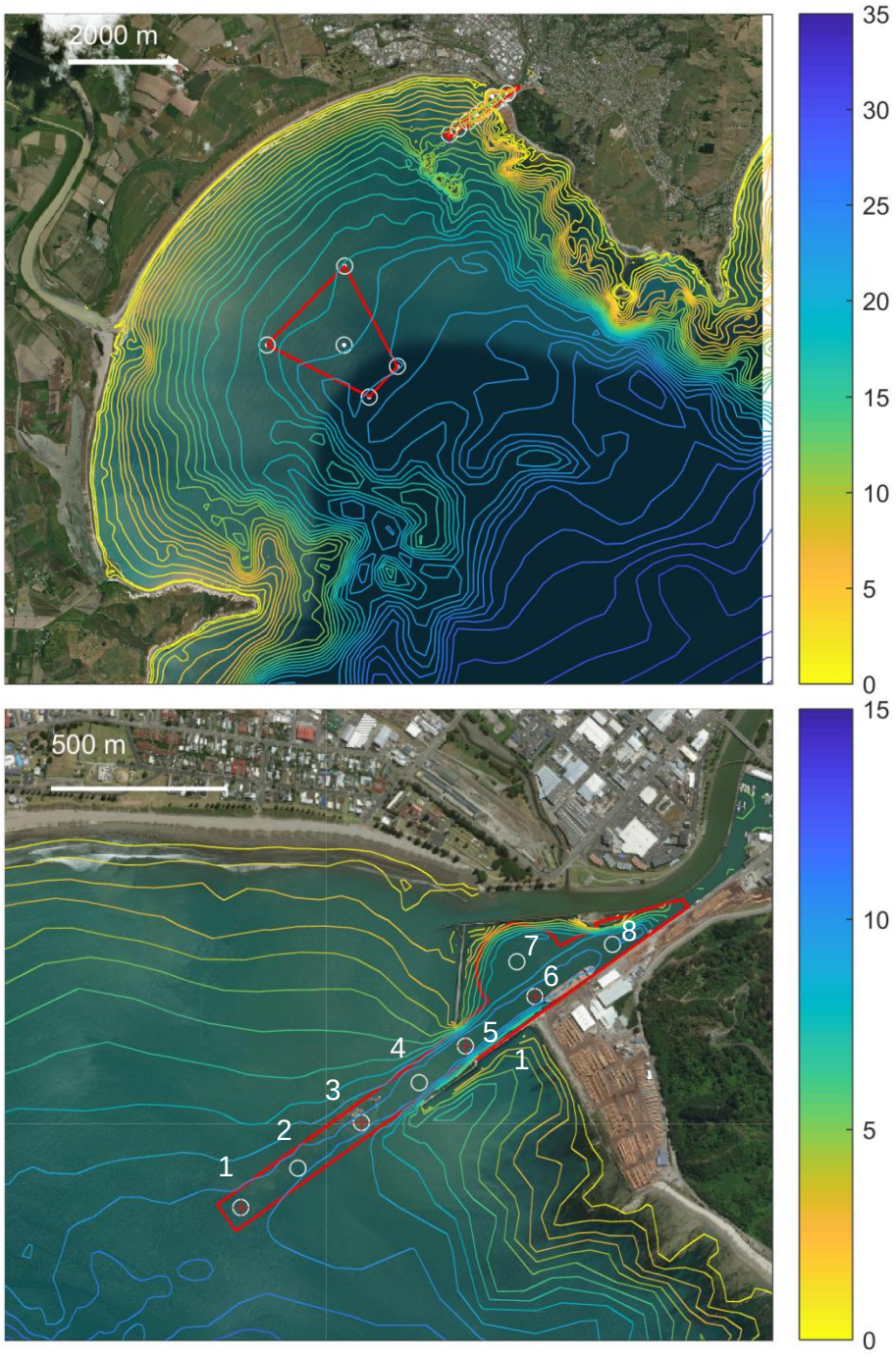

Figure 2-1 Release sites considered for the sediment dredging (white circles). The extents of the disposal ground and channel are shown in red.

2.2. Hydrodynamics

The particle-tracking simulations reproducing the dredging operations were undertaken using a 3D hydrodynamic hindcast simulated with the unstructured-grid

finite-element SCHISM model[1][2]. Note the same dataset was used in the disposal plume modelling (MetOcean Solutions, 2018).

SCHISM is a prognostic finite-element unstructured-grid model designed to simulate 3D baroclinic, 3D barotropic or 2D barotropic circulation. The barotropic mode equations employ a semi-implicit finite-element Eulerian-Lagrangian algorithm to solve the shallow-water equations, forced by relevant physical processes (atmospheric, oceanic and fluvial forcing). A detailed description of the SCHISM model formulation, governing equations and numerics, can be found in Zhang and Baptista (2008).

In the present implementation, SCHISM was run in 3D mode using a combination with a vertical discretization using *Localized Sigma Coordinate system with Shaved Cell* (LSC2) which is type of terrain-following layers as described in Zhang et al. (2015). The number of vertical layers ranged from 4 in shallow waters to 12 in deep waters near the open boundary. On the horizontal space, the finite-element triangular grid structure used by SCHISM has many advantages over the regular or curvilinear grid structure with respect to the representation of complex shoreline and bathymetric features (port channel and structures, reefs and shoals). Here, the horizontal resolution ranged from 150 m at the offshore boundary to 5 m in shallow water. The model domain was also refined around key features, including within Eastland Port, along the shipping channel, within the associated river systems and in areas with complex topography (i.e. Tokomaru, Hawea and Temoana Rocks and the rocky reef shore line). The triangular elements of the model domain meshes are shown in Figure 2-2 and associated bathymetries are presented in Figure 2-3.

This high-resolution SCHISM 3D model was nested within a downscaled 3D hydrodynamic hindcast of the wider Poverty Bay region simulated using the Regional Ocean Modelling System (ROMS). This *parent* Poverty Bay ROMS model provided 3D initial and boundary conditions to the SCHISM domain over the two annual periods considered El Niño (2002-2003) and La Niña (1998-1999) periods.

The full details and validation of the 3D ROMS hindcast and downscaling approach from a New Zealand wide domain (resolution 8km) to the Poverty Bay domain (resolution 150m) are provided in report P0331-04 (MetOcean Solutions, 2017).

[1] http://ccrm.vims.edu/schism/
[2] http://www.ccrm.vims.edu/w/index.php/Main_Page#SCHISM_WIKI

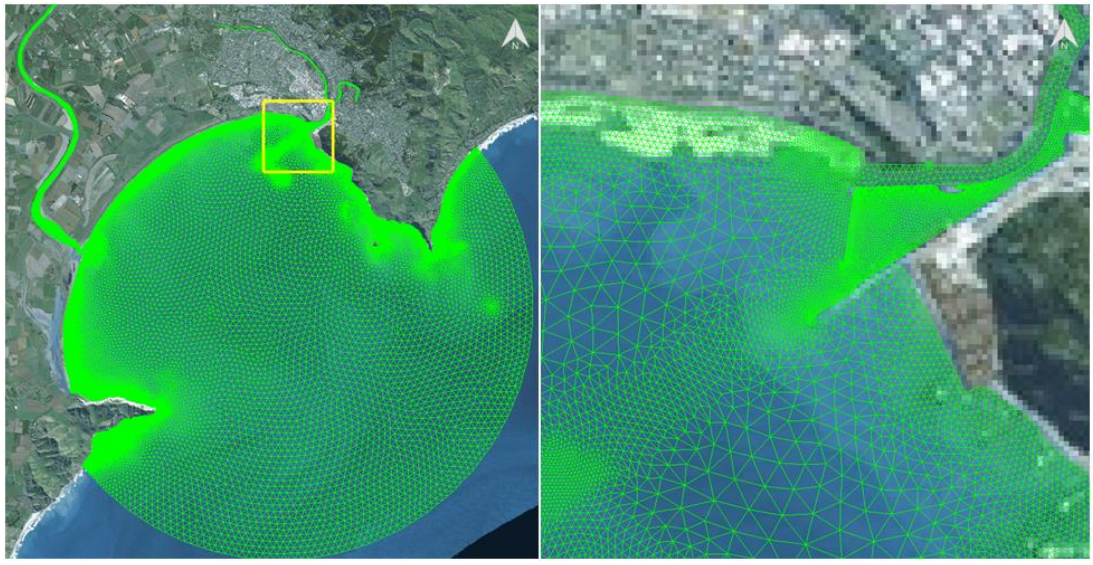

Figure 2-2 Unstructured mesh-grid used in SCHISM to simulate the hydrodynamics over Poverty Bay (left) and Eastland Port (right).

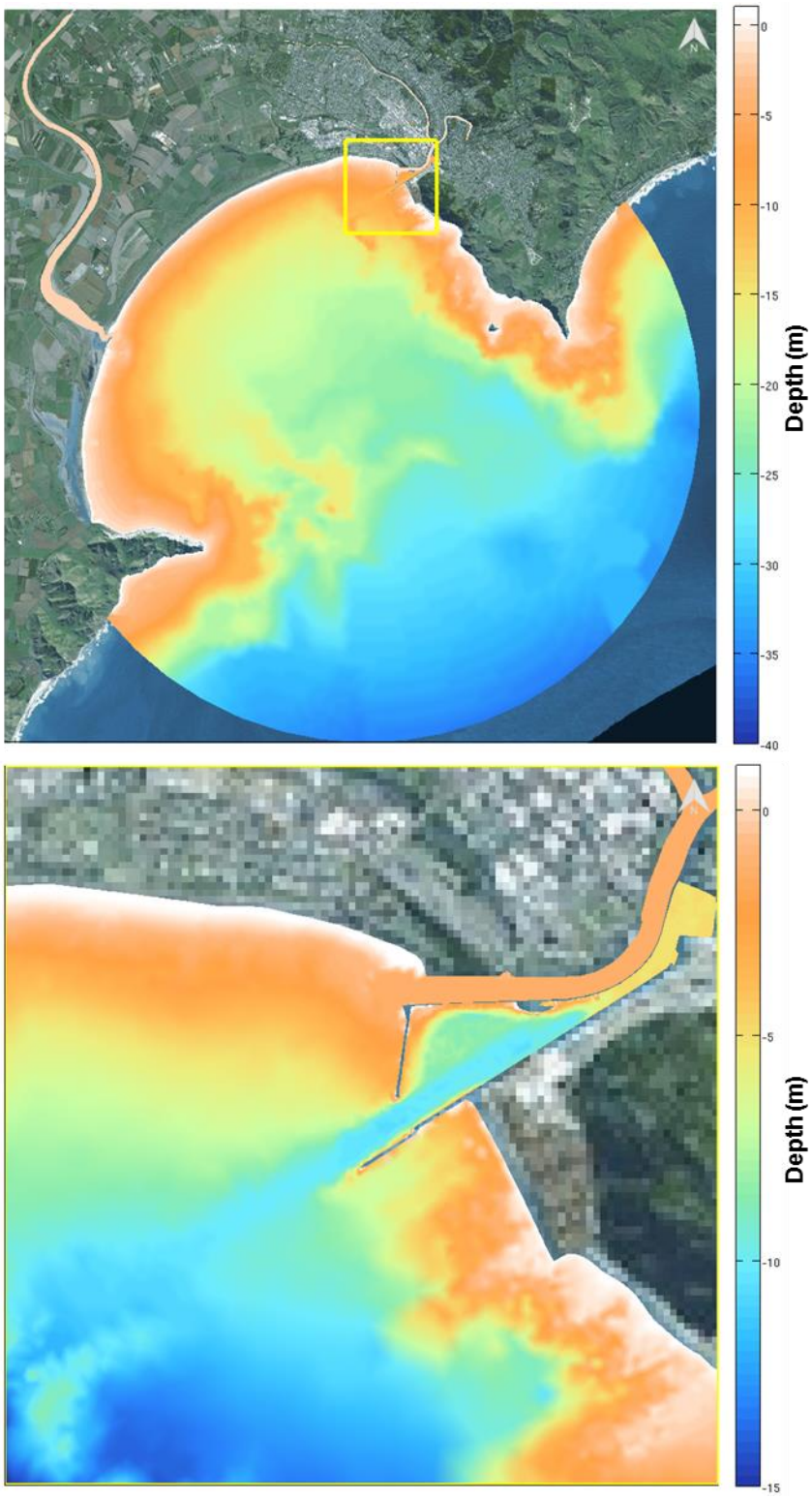

Figure 2-3 Model bathymetries (below mean sea level) over Poverty Bay (left) and Eastland Port (right).

2.3. Trajectory modelling

2.3.1. Particle-tracking model

A Lagrangian model developed by MOS was used to simulate the trajectories of particles released at the dredging sites. Here, the particles represent the sediment discharged from the dredging vessel.

The model consists of trajectory scheme applied to the 3D Eulerian current field $(\tilde{u},\tilde{v})$, solving for the motion of discrete particles.

$$\frac{dx_p}{dt} = \tilde{u}(x,y,z,t) + u_t$$
$$\frac{dy_p}{dt} = \tilde{v}(x,y,z,t) + v_t \qquad \text{(2.1 a,b,c)}$$
$$\frac{dz_p}{dt} = -w_s + w_t$$

where (x_p,y_p,z_p) are the particle coordinates, (u_t,v_t,w_t) are the diffusion components representing turbulent motions, w_s is the particle settling velocity.

In the horizontal plane, the model uses an Ordinary Differential Equations (ODE) solver, including a 4th order Runge-Kutta method, to calculate the trajectory of a given particle (x_p,y_p) in the time-varying current field.

In the vertical plane, particle motion is controlled by the specified settling velocity w_s, as well as the vertical diffusion component w_t as defined in equation 2.1c.

Horizontal and vertical diffusion motions are treated with the following equation, shown here for the u_t component:

$$\int_t^{t+\Delta t} u_t . dt = \sqrt{6 . k_{u,v} . \Delta t} \; . \theta(-1,1) \qquad (2.2)$$

where $\theta(-1,1)$ is a random number from a uniform distribution between -1 and 1, Δt is the time-step of the model in seconds and $k_{u,v}$ is the horizontal eddy diffusivity coefficient in $m^2.s^{-1}$. The same equation is used for the vertical diffusion.

In absence of specific field data on diffusive processes, the determination of the eddy diffusivity coefficient $k_{u,v}$ is generally based on guidance from empirical relationships. Several relationships are summarized in Fischer et al. (1979) including that of Elder (1956) for simple unidirectional shear flows that estimates the longitudinal diffusion coefficient as a function of the water depth and current velocity of the form.

$$k_{u,v} = 5.93 . H . u^* \qquad (2.3)$$

where H and u^* are the water depth and friction velocity respectively.

Transverse mixing can be estimated using a relationship of the same form but with reduced proportionality factor (with 50 % error bound).

$$k_{transverse} \sim 0.6 . H . u^* \qquad (2.4)$$

The vertical eddy diffusivity is generally expected to be at least one order or magnitude smaller. Elder's formula suggests a vertically averaged value of:

$$k_{vertical} \sim 0.067.H.u^{*} \quad (2.5)$$

Here, both depth and mean current velocities vary throughout the region of interest but these equations can still be used to provide a bracketing of reasonable eddy diffusivity coefficient values for the present application.

Assuming a generic water depth of order 10.0 metres in the channel region and using mean current velocities of ~ [0.02-0.5] $m.s^{-1}$ at the outer end, port entrance and inner basin respectively, the above equations yield average horizontal coefficients (i.e. average of longitudinal and transverse results) in the range [0.3-0.8] $m^2.s^{-1}$.

Furthermore, in numerical models, the role of the horizontal diffusion coefficient is also to implicitly account for sub-grid scale turbulent processes such as eddies that are not explicitly resolved in the model due to the limited resolution. This means that horizontal diffusion must generally increase as grid size increases since eddies of increasing scale are unrepresented. On the contrary, the reduction of grid size allows explicit resolution of flow patterns and eddies at finer scales, which thereby reduces the required amount of added diffusion.

For dispersion at oceanic scales, (Okubo, A., 1971) notably showed that $k_{u,v}$ varies approximately (with wide scatter) as :

$$k_{u,v} = \alpha.L^{4/3} \quad (2.6)$$

where L is the horizontal scale of the mixing phenomena and α is an empirical proportionality factor.

The model mesh has fine spatial resolution throughout the channel region of order 30-50 m which yields average horizontal diffusivities of [0.025-0.05] $m^2.s^{-1}$.

Here a generic value of 0.05 $m^2.s^{-1}$ was eventually chosen for the horizontal eddy diffusivity. The value is smaller than the one used for the disposal modelling due to the finer grid resolution used here.

The vertical eddy diffusivity is expected to be significantly smaller than the horizontal magnitude; it was set to a small generic value of 0.0001 $m^2.s^{-1}$ to ensure that the vertical settling of disposed sediment was not overly altered by the vertical diffusion.

Finally, in the present model implementation, any particle reaching the shoreline, or the seabed was removed (i.e. sticky boundaries).

2.3.2. Sediment distribution and settling velocity

The dredging simulations require the definition of a set representative sediment particle classes, which will settle at different velocities, representing the different fractions of the sediment material to be dredged.

The sediment distribution used for the dredging plume modelling was the same as the one used for the disposal plumes (MetOcean Solutions, 2018). The description of the sediment distribution is reproduced below for convenience.

Some information on the surficial sediment distribution within the port basin and outer bay are available in Beamsley (2003), and summarized in Table 2.1. These results shows the presence of both fine sand and finer cohesive sediments (i.e. d_{50}<63 µm), with varying distribution throughout the region.

Although general equations are available to compute the settling velocity of individual particles of given sizes (e.g. Stokes Law), it is unrealistic to assume that the sediment consists in single particles in the fine silt range (~63 µm or smaller) because of the cohesive nature of material and associated flocculation effects (i.e. formation of particle aggregates) (e.g Van Rijn, 2007).

In the absence of in-situ measurements on the settling of such flocculated cohesive sediment at the site, a "cohesive sediment class" with generic settling rate of 1 $mm.s^{-1}$ was initially used, which is appropriate for such flocculated particles (Whitehouse R. et al., 2000), and commonly used in the context of sediment disposal (e.g. Smith and Friedrichs, 2011) to represent the finest sediment grain size fraction. Simulations were then reproduced using a smaller settling rate of 0.1 $mm.s^{-1}$ to assess the effects of slower sediment settling on the resulting *ssc* plume footprints.

The sandy fraction of the material to be disposed was represented using a "sand class" with a settling velocity of 8 $mm.s^{-1}$, which is equivalent to the theoretical settling velocity associated with the smallest sand median diameter of Table 2.2 (110 microns). Note the smallest sand diameter present was chosen for conservatism; some of the sandy material may indeed be coarser than this generic diameter and thus settle faster.

The relative distribution of cohesive versus sandy material is seen to significantly vary throughout the region of interest, from the channel basin (80%-20%) to the outside of the port (20%-80%) (see Table 2.1). Note the fine cohesive sediment is the most problematic with respect to the produced sediment plumes since it remains much longer in suspension in the water column.

In the present applications, these two contrasting sediment distributions were considered assuming that the sediment to be dredged at sites 1 to 4 (outer channel) would be mostly sand i.e. 80 % sand, 20% silt, and while that at sites 5 to 8 (inner basin) would be mostly silt, i.e. 20% sand, 80% silt (see Figure 2-1 for sites positions).

Beamsley (2003) reports a sediment wet bulk density of 1892 $kg.m^{-3}$, with a moisture rate of 40 %, on the outer channel region (site SS). This yields a dry bulk density of ~1350 $kg.m^{-3}$. The inner basin (site SB), which includes a larger fraction cohesive material, has a smaller wet bulk density of 1381 $kg.m^{-3}$ with a high moisture content of 110 % which yields a dry bulk density of ~650 $kg.m^{-3}$.

Table 2.1 Surficial sediment distribution within the port basin and outer bay (Beamsley, 2003).

	Percentage	**Median diameter d50**
Inner Basin	**[%]**	**[microns]**
sand	20%	180
silt	60%	20
clay	20%	2
Channel Entrance		
sand	80%	170
silt	10%	20
clay	10%	2
Outside of Port		
sand	70%	110
silt	20%	30
clay	10%	2

Table 2.2 Settling velocities, and relative distribution of the representative cohesive and sand sediment classes for dredging sites 1 to 4. A dry density of 1350 kg.m^{-3} was assumed based on samples in Beamsley (2003) (site SS).

	Settling velocity	**Percentage**
Sandy sediment class	8 mm.s^{-1}	80 %
Cohesive sediment class	[0.1 and 1] mm.s^{-1}	20 %

Table 2.3 Settling velocities, dry density and relative distribution of the representative cohesive and sand sediment classes for dredging sites 5 to 8. A dry density of 650 kg.m^{-3} was assumed based on samples in Beamsley (2003) (site SB).

	Settling velocity	**Percentage**
Sandy sediment class	8 mm.s^{-1}	20 %
Cohesive sediment class	[0.1 and 1] mm.s^{-1}	80 %

2.3.3. Sediment dredging processes and source terms

The processes by which sediment is released and suspended in the water column during dredging operations are briefly outlined in the context of the choice of the source term magnitudes and release depths for the particle tracking simulations undertaken in this study.

The dredging method considered involves the use of the Pukunui vessel which is a Trailing Suction Hopper Dredger (TSHD) with a hopper capacity of 480 m^3. It is also possible that backhoe dredging will be used in the inner port basin where TSHD use is not feasible. General dredger details are provided in Table 2.5.

During the TSHD dredging phase (see Figure 2-4), sediment is sucked into the vessel hopper using a drag head; a fraction of the sediment disturbed by the drag head is not pumped into the hopper and remains suspended in the water column. Sediment suspension is also expected due to the action of propeller wash. These two sources of sediment suspension are identified as sources 1 and 3 in Figure 2-4.

In the present study the following sediment releases were used for these sources :

- Drag head source: bottom 3 meters of water column.
- Propeller wash source: bottom 3 m of the water column.

After the initial hopper infilling, the actual content of the hopper is a sediment/water mixture which is expected to contain ~20 % solids by volume (Spearman et al., 2007). To maximize the amount of sediment in the hopper, it can be decided to continue to pump sediment and water from the seabed; this will result in the hopper "overflowing" and thereby releasing some sediment in the water column. The overflow releases generally occur through pipes in larger TSHD but can be simply released on deck and overboard on smaller vessels like Pukunui. This phase will be referred to as "overflow phase", and is shown as the source "2" in Figure 2-4.

The overflow load consists of a highly concentrated mixture of sediment and water and the bulk behavior of that sediment mixture may become dominant over the individual particle settling processes (Winterwerp, J.C., 2002).

When the overflow mixture is released through pipes, it is expected that the overflow release will be followed by a dynamic plume phase where the sediment mixture descends to bottom as a jet-like feature, and impacts the seabed, suspending sediment and forming an initial density driven near-bed plume. A fraction of the sediment load will be de-entrained from the dynamic plume during descent and become suspended in the water column. This is comparable to processes involved during the offshore disposal i.e. 1) Convective descent, 2) Dynamic Collapse, and 3) Passive plume dispersion (see Figure 2-6).

The general length scales expected for the overflow process are an order of magnitude smaller than the discharge of sediment at the offshore disposal ground. Additionally, the overflow sediment mixture is less concentrated than in offshore sediment disposal context.

In the present case, this overflow phase was modelled considering two sources of sediment to the passive plume:

- Suspension of sediment de-entrained from the dynamic plume descent uniform release within the entire water column, and

- Passive plume generated following the dynamic plume impact: release within a cylinder of 2 m height and 60 m radius on the seabed.

This dynamic plume formation is less likely when the overflow is initially released over the deck and then flowing overboard, as for the Pukunui vessel (Figure 3-9), given the reduced downward momentum and density of the released sediment mixture. In that situation, the overflow release is relatively diffuse and was considered as:

- Overflow diffuse source: surface 3 meters of water column.

For the dredging of the inner port basin where dredging vessels may not be able to manoeuver properly, it is possible that some dredging will be undertaken using a backhoe dredger (see Figure 2-5). In that configuration, sediment is removed from the seabed using a backhoe arm, with a bucket at the end, and the sediment is then placed onto the vessel hopper. The backhoe source term was considered as:

- Backhoe source: cylinder of 32 m radius (i.e. radius of backhoe arm), spread across the entire water column.

For conservatism, an additional source reproducing the possible sediment surface loss was also included in the simulation.

- Surface loss source: surface 2 meters of water column

The sediment fractions to be applied to the different source terms recommended in Becker are reproduced in Table 2.6. The fractions applied to the different source terms in the present applications are summarized in Table 2.7.

The dredging scenarios considered, which account for the different dredging methods (Pukunui and backhoe dredger), operating modes (i.e. overflow versus no overflow), as well as different positions within the port basin and channels (and thus sediment distribution), are listed below.

- Dredging with Pukunui in the outer channel, with no overflow (sites 1-4)
    - Predominant sandy material (80% sand, 20% silt)
    - Drag head and propeller wash
    - Surface losses
- Dredging with Pukunui in the outer channel, with overflow (sites 1-4)
    - Predominant sandy material (80% sand, 20% silt)
    - Drag head and propeller wash
    - Surface losses
    - Diffuse overflow
- Dredging with Pukunui in the inner port, with no overflow (sites 5-8)
    - Predominant silty material (20% sand, 80% silt)
    - Drag head and propeller wash
    - Surface losses
- Dredging with Pukunui in the inner port, with overflow (sites 5-8)
    - Predominant silty material (20% sand, 80% silt)

  - Drag head and propeller wash
  - Surface losses
  - Diffuse overflow

- Dredging with backhoe dredger in the swinging basin/berth8 region (sites 5-8)

  - Predominant silty material (20% sand, 80% silt)
  - Backhoe losses

The magnitudes of the various sources terms were defined using methods described in Becker J. et al.(2015). In his approach, source term magnitudes, are estimated based on the expected *dredger production rate* which is the amount of in-situ sediment removed per unit time ($m^3.s^{-1}$). The productions rates which are used as inputs to the methods were defined from information provided by Eastland Port Limited.

The amount of sediment transferred to the passive plume by each source term (in $kg.s^{-1}$) is then defined as a fraction of the *dredger production rate*. Some empirical ranges for the source terms fractions are provided in Table 2.6. For example, the drag head disturbance is expected to be order 0 to 3 % of the effective production rate, while the amount of sediment de-entrained from the released overflow is expected to be of order 0-20%, while the rest is found in a nearbed density current. Note that, for conservatism, we applied the source term estimation approach to both the cohesive and sand fractions, while Becker J. et al.(2015) 's method only consider the cohesive fractions (i.e. fines) given the rapid settling of sand.

The release sites considered for the dredging are shown in Figure 2-1 (positions in Table 2.4). All the individual source terms modelled at each site are summarized in Table 2.7. The details of the different source terms used for each dredging scenarios are included in Appendix A.

Note that the simulations have assumed static sediment release at each site considered, for conservatism. In reality the moving dredge will allow some dilution of the plumes as it moves, particularly on the outer channel region, and the results should thus be interpreted as worst-case footprints. For comparison, the relative plume spreading for a moving dredger is illustrated based on 7-day simulations reproducing a vessel navigating along the outer channel (back and forth from site 1 to site 5 along the channel centerline, see Figure 2-1).

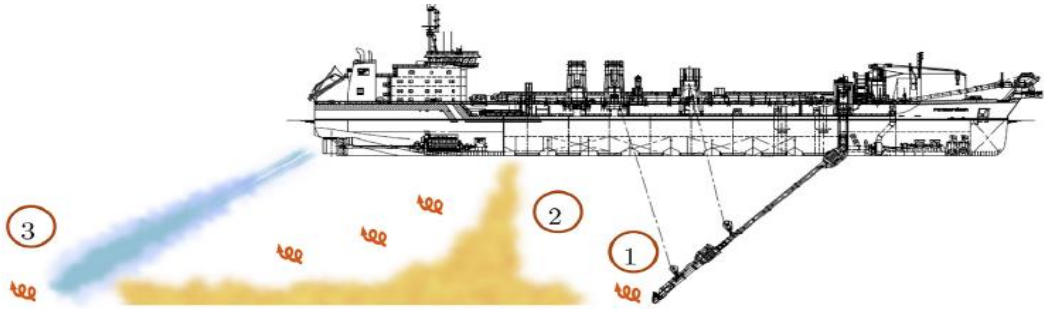

Figure 2-4 Sediment suspension sources of a dredge plume for a Trailing Suction Hopper Dredger: 1-Drag Head, 2-Overflow, including de-entrainment during plume descent through the water column and density current on the seabed, 3-Propeller wash (from Becker J. et al., 2015).

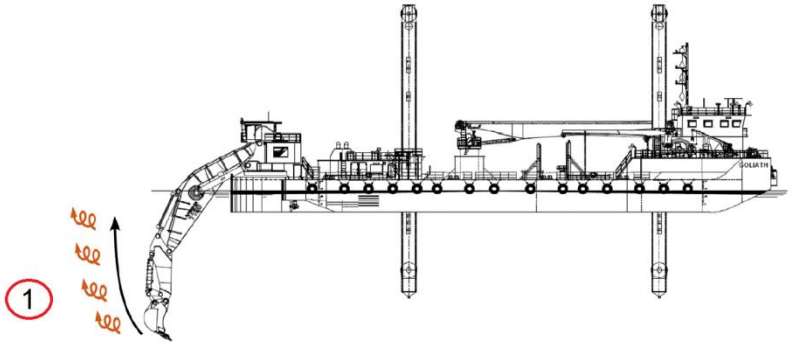

Figure 2-5 Sediment suspension sources of a Backhoe Dredger (from Becker J. et al., 2015).

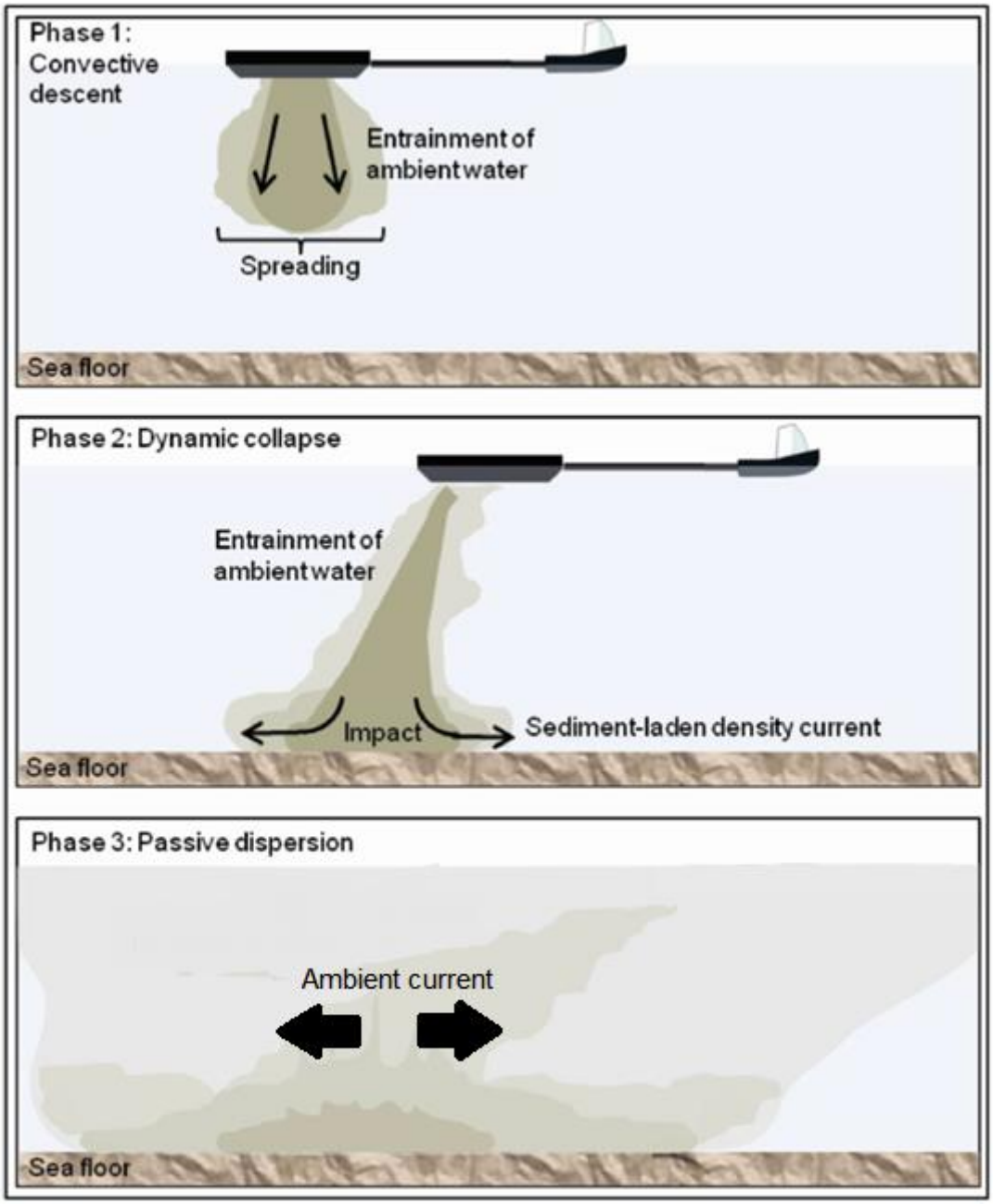

Figure 2-6 Three main phases occurring during the disposal of dredged material: 1) Convective descent, 2) Dynamic Collapse, and 3) Passive plume dispersion. Similar processes are expected when dense overflow sediment mixture is released during dredging.

Table 2.4 Coordinates of release sites considered along the channel.

	Longitude	Latitude
channel_1	178.0127	-38.6806
channel_2	178.0146	-38.6796
channel_3	178.0166	-38.6785
channel_4	178.0185	-38.6775
channel_5	178.0200	-38.6765
channel_6	178.0223	-38.6753
channel_7	178.0217	-38.6744
channel_8	178.0248	-38.6740

Table 2.5 General details of Pukunui vessel.

Vessel	PUKUNUI
Length	36.58m
Draft - empty	1.2 m
Draft - full	2.4 m
Hopper Volume	480 m^3

Table 2.6 Reasonable ranges for (empirical) source term fractions (from Becker J. et al., 2015).

Plume source	Symbol	Fraction
Draghead	σ_d	0–0.03
Overflow ratio	R_o	0–1
In-hopper settlement	f_{sett}	0–1
In-matrix fixation	f_{trap}	0.01–0.05
Overflow	σ_o	0–0.2
Cutterhead	σ_c	0.01–0.05
Bucket drip	σ_b	0–0.04
Bottom door (hydraulic)	σ_p	0–0.1
Bottom door (mechanic)	σ_p	0.0–0.05

Table 2.7 Summary of all source terms simulated

Source terms	Release depth	Radius	Fraction
Overflow (sediment de-entrained during descent)	water column	point	0.2
Overflow (density current at the bottom)	bottom 3m	60 m	0.8 (1-0.2)
Overflow (diffuse release - Pukunui)	surface 3m	point	0.2
Propeller wash	bottom 3m	point	0.015
Drag head disturbance	bottom 3m	point	0.015
Backhoe (bucket losses)	water column	37 m	0.04
Surface sediment losses	surface 2m	point	0.01

2.4. Post-processing

2.4.1. Concentration and depositional thickness computation

A Lagrangian model outputs a set of particles positions changing over time, thus describing their trajectories. However it is often needed to reconstruct particle concentration fields, which is a more quantitative metric to assess actual suspended sediment concentration levels, or depositional thickness.

The “concentration” of particles at a given point (x,y,z) is obviously related to the particle “density” in the region surrounding this point. Historically, the calculation of concentration at a receptor (x,y,z) in Lagrangian particle models has been made by the so-called *box-counting* technique. The technique consists in counting the number of particles within a “box” that is centred on the receptor and then dividing the total mass of the particles by the box volume (Bellasio, et al., 2017).

The approach has important limitations; since concentration computed in boxes containing a small numbers of particles are affected by relatively large statistical errors, simulations generally need to include a large number of particles to obtain an acceptable resolution in the computed concentration field (Vitali et al., 2006). Furthermore, a compromise needs to be made on the dimension of the boxes so that they are large enough to include a statistically significant number of particles and thus yield a continuous concentration field, but not too large so that the concentration field is not over-smoothed (e.g. Bellasio, et al., 2017). This relatively arbitrary choice can have important effects on the resulting concentration field magnitudes (De Haan, 1999). The method is beside very computationally expensive.

An alternative, more robust, numeric technique for computing concentrations fields from Lagrangian particles is the *kernel density estimator* (Silverman, 1986). In the kernel density approach, individual particles are assumed to represent the centre of mass of a “cloud”; the density profile of the cloud is described by the *kernel function*, while the spreading of the particle’s equivalent mass is defined by the *bandwidths* associated with a given particle or receptor (Bellasio, et al., 2017; Vitali et al., 2006). These two components are then used to derive a *particle density field*, also referred to as a *probability density function*.

Here, the kernel density estimation is undertaken following the approach proposed by Botev, et al. (2010). The proposed method uses an adaptive kernel density estimation method based on the smoothing properties of linear diffusion processes. The key idea is to view the kernel from which the estimator is constructed as the transition density of a diffusion process (Botev, et al., 2010). Their methods limit the amount of guessing on the original data, notably to define bandwidths, as well as possible excessive smoothing of the density fields (e.g. as obtained with Gaussian kernel density estimators). The kernel density estimations algorithms for both one and two dimensional spaces have been implemented in Matlab by the authors themselves[3] [4], and these have used in the present study.

Based on a given cloud of particles (X_{part},Y_{part}), the method yields a *probability density function PDF(x,y)*, derived from the *kernel density estimator* describing the density of particles throughout the domain. The spatial integration of the *probability density function PDF(x,y)* over the entire domain equals to one.

[3] https://fr.mathworks.com/matlabcentral/fileexchange/17204-kernel-density-estimation
[4] https://fr.mathworks.com/matlabcentral/fileexchange/14034-kernel-density-estimator

$$\sum_i^n PDF(x,y) \,.\, dx \,.\, dy = 1 \qquad (2.7)$$

where n is the number of receptors, and (dx,dy) are the dimensions of the grid cells for which the PDF is computed.

The *PDF(x,y)* is provided over a rectangular grid with a resolution that can be adjusted by the user.

The *PDF(x,y)* values can be converted to particle density when timed by the total number of particles in the domain i.e. with units [particles.m^{-2}]. The particle density can in turn be converted to mass density, or mass distribution, based on the equivalent mass carried by individual particles i.e. with units [mass.m^{-2}]. Mass concentration (i.e. *ssc*) is obtained by dividing the mass density by the water depth i.e. with units [mass.m^{-3}].

A similar approach can be followed for estimating the depositional thickness. The probability density function of the deposited particle is computed and converted to a sediment mass density field in [mass.m^{-2}]. Using the known density allows determining the sediment volume deposited per m^2, which effectively yields the deposition thickness i.e. [m^3.m^{-2} = m].

2.4.2. Application to present study

In the present study, the results of the two different 1-year long simulations (El Niño, La Niña) were post-processed to produce probabilistic footprints of the *ssc* field footprints. The probabilistic approach consists in combining the entire dataset of particle trajectories predicted throughout each year, under a wide range of ambient current forcing, and computing the associated suspended sediment concentration (*ssc*) and sediment depositions fields.

This allows identifying the key dispersion pathways from each release site and assessing expected *ssc* magnitudes. Here, presented *ssc* fields results should be interpreted as equilibrium states that would develop at each cycle once the dredging vessel has been operating for sufficient time.

Results are presented for the Pukunui TSHD vessel as well as the backhoe dredger in the port basin. Vessel details are summarized in Table 2.5.

The KDEs and resulting *ssc* fields for the probabilistic cases (i.e. combining all outputs) were computed over a grid of 256 by 256 cells, centred on each release site, with a spatial resolution of (dx,dy) of ~ 15 m, within three different layers of the water column, namely surface, mid-depth and bottom. Each layer is 3 m thick.

Note that the presented *ssc* fields do not include the natural ambient *ssc*, which may be significant in the Bay, and in the vicinity of the port due to wave generated drift, and nearby river discharges (e.g. see Beamsley, 2003).

3. RESULTS

3.1. Hydrodynamics

The distribution of the total currents at the sites 1, 3, 5, and 6 along the channel (Figure 2-1), at three levels in the water column are shown in Figure 3-1 to Figure 3-7 for the El Niño and La Niña annual periods.

In general, current regimes over the two annual periods considered are very similar. The outermost site 1 shows a bi-modal current distribution, with dominant north and southeast directions. The southeast component is strongest at the surface (up to 0.3m.s^{-1}) and weakens deeper in the water column; the bottom currents are weak of order 0-0.1 m.s^{-1}, with a dominant north component.

At site 3, surface currents are predominantly south-directed (i.e. across the entrance). The south-directed component is still present at mid-depth though counterbalanced by some north-directed currents as well. Bottom currents are weak and northeast-directed.

Currents expectedly align with the channel orientation at sites 5 and 6. These show some possible stratification of the water column with contrasting dominant directions; bottom current are consistently northeast directed while a strong southwest component is present at mid-depth. This may be related to the ocean and river water masses whereby the denser seawater stays below the lighter freshwater from the river.

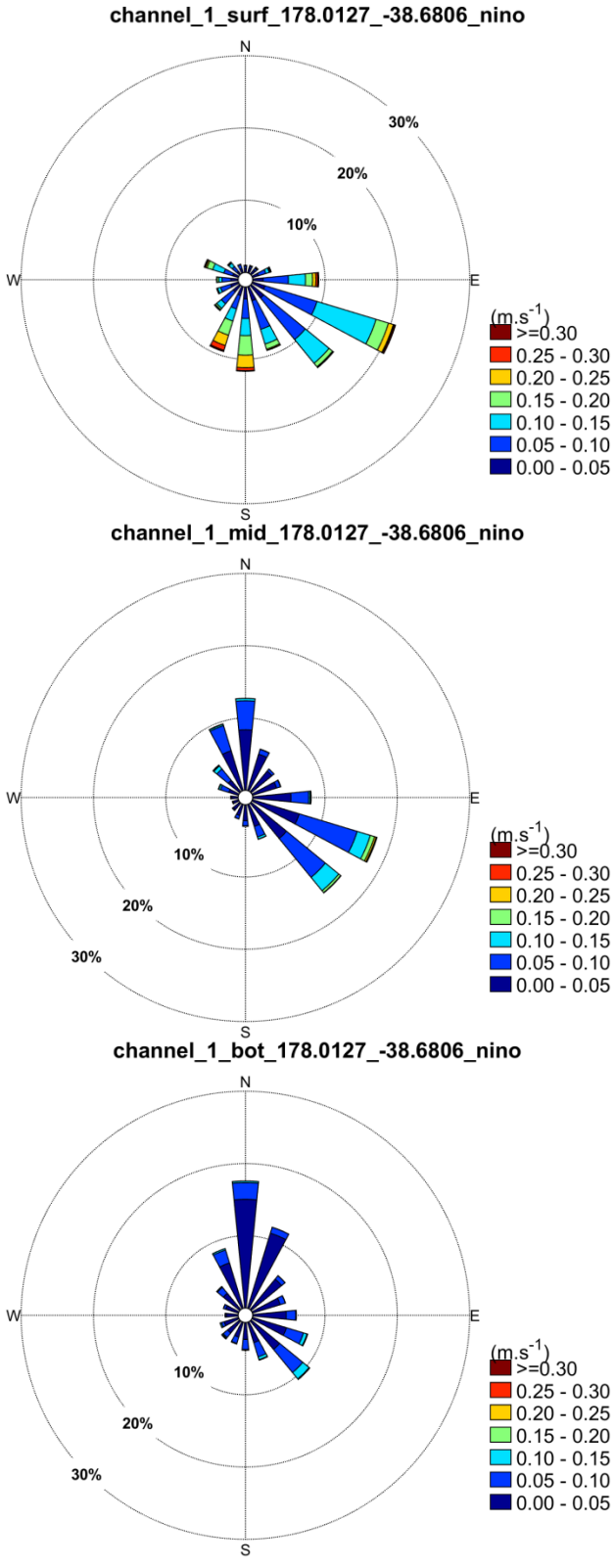

Surface

Mid depth

Bottom

Figure 3-1 Annual current roses of surface, mid-depth, and bottom currents at site 1 for the El Niño period (June 2002- June 2003) (see Figure 2-1 for position).

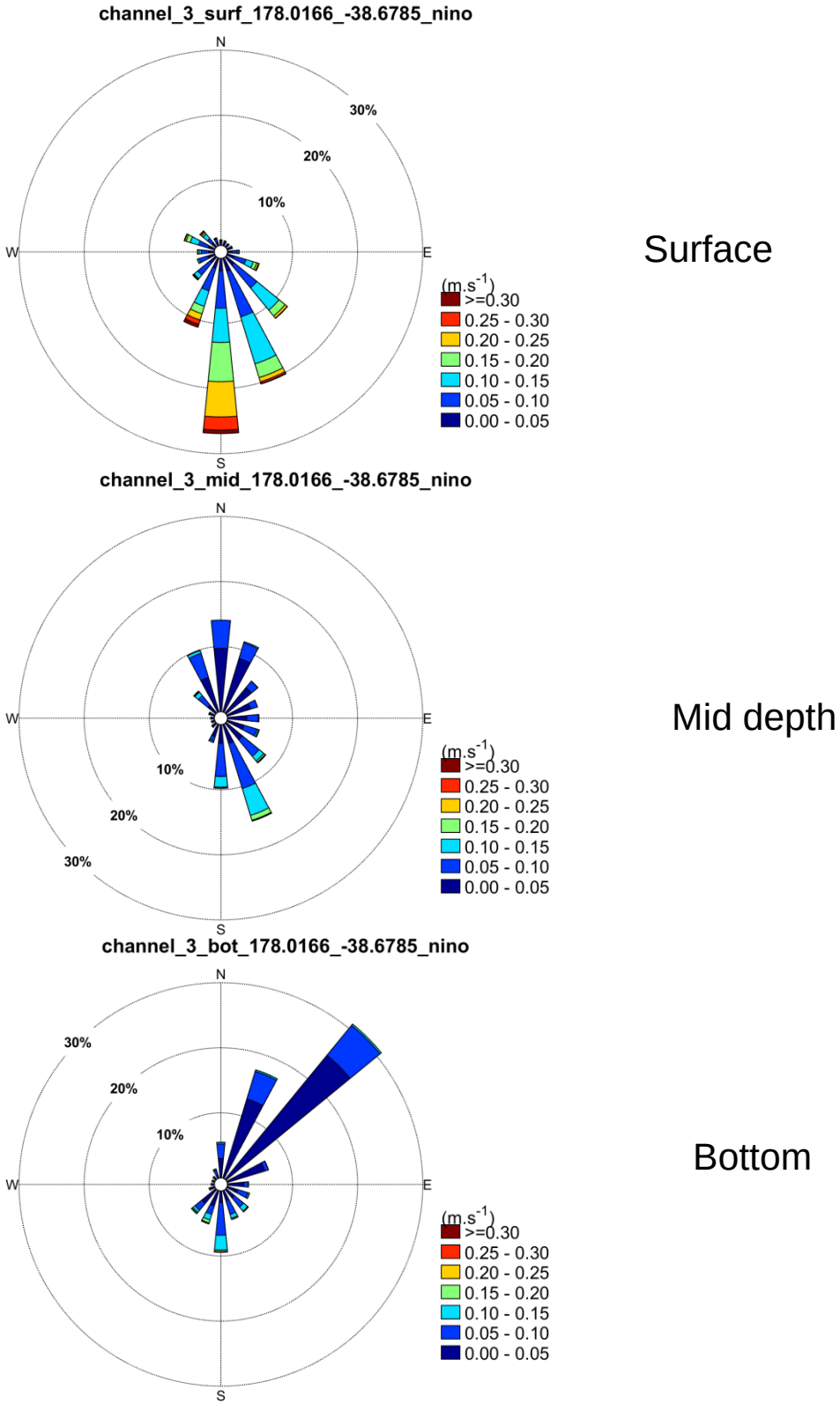

Figure 3-2 Annual current roses of surface, mid-depth, and bottom currents at site 3 for the El Niño period (June 2002- June 2003) (see Figure 2-1 for position).

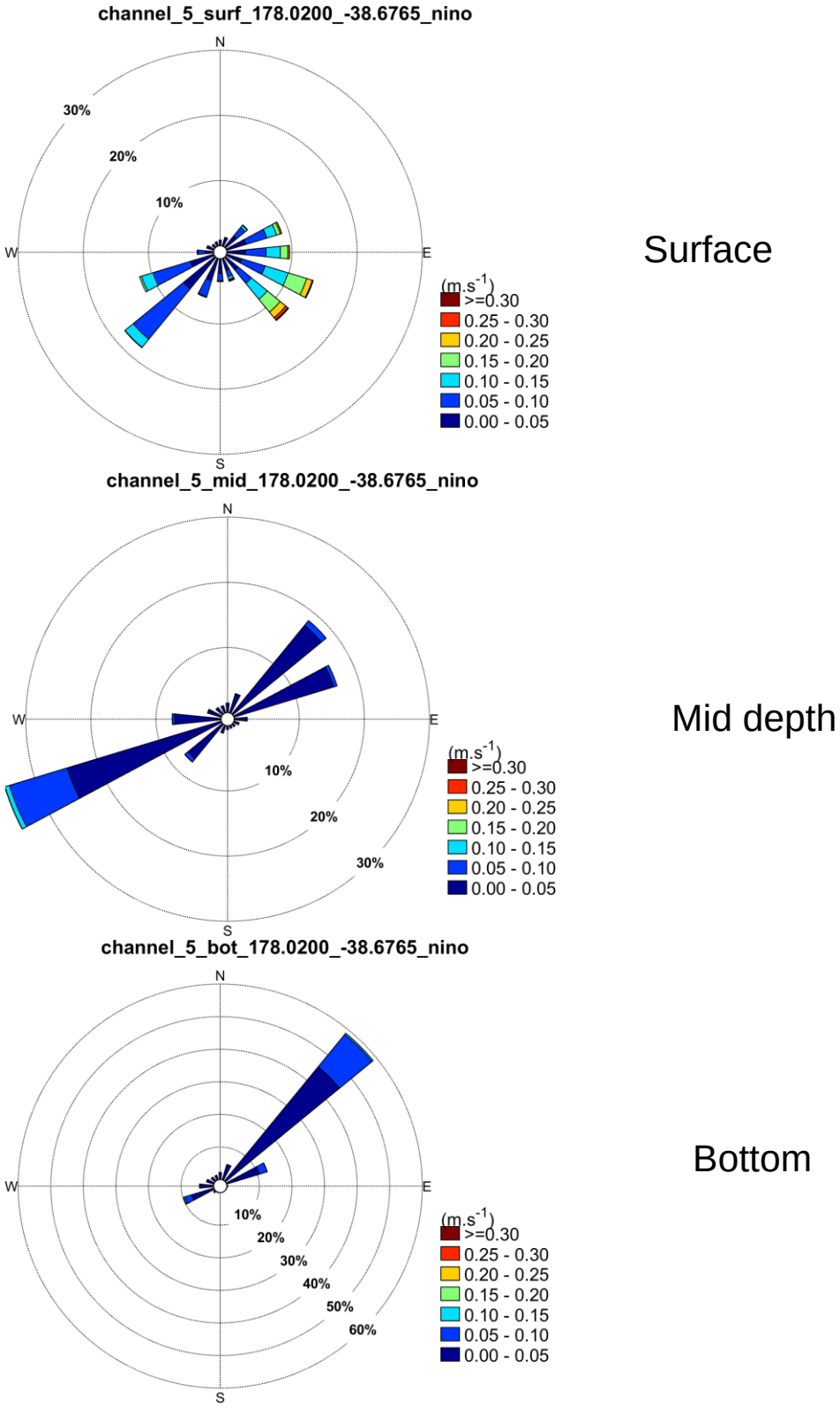

Figure 3-3 Annual current roses of surface, mid-depth, and bottom currents at site 5 for the El Niño period (June 2002- June 2003) (see Figure 2-1 for position).

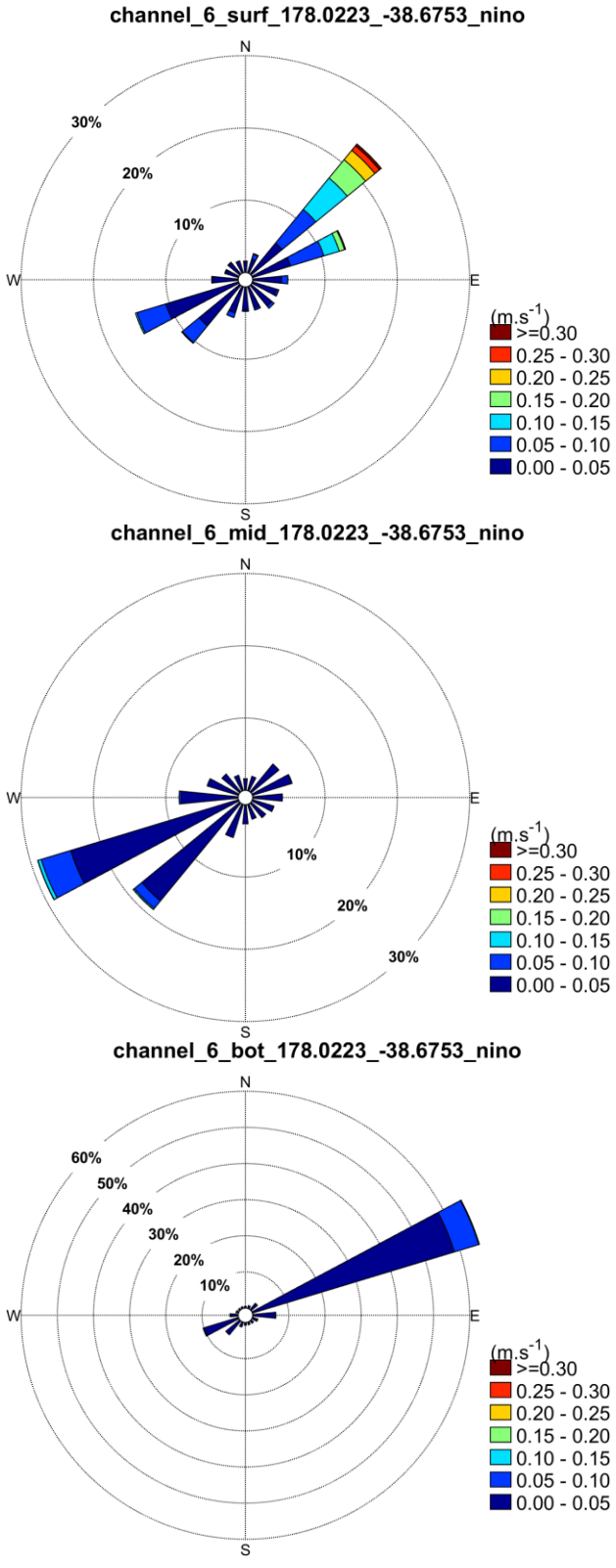

Surface

Mid depth

Bottom

Figure 3-4 Annual current roses of surface, mid-depth, and bottom currents at site 6 for the El Niño period (June 2002- June 2003) (see Figure 2-1 for position).

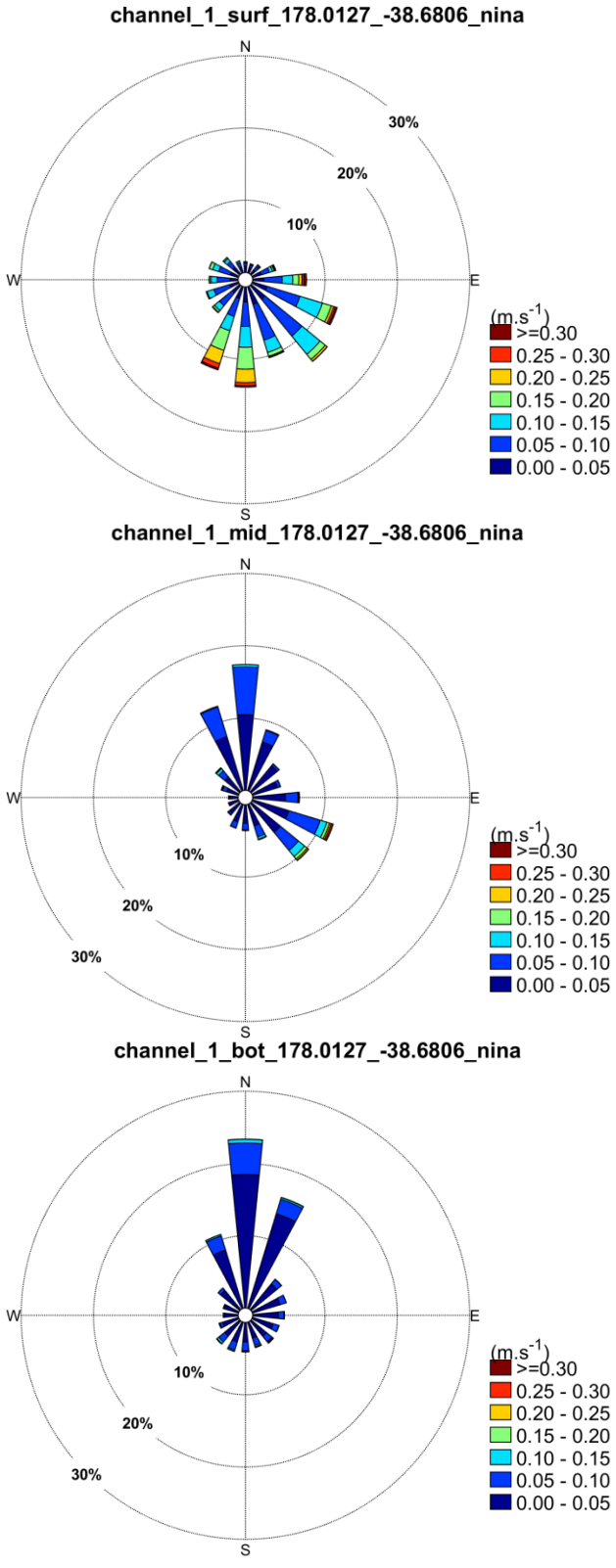

Surface

Mid depth

Bottom

Figure 3-5 Annual current roses of surface, mid-depth, and bottom currents at site 1 for the La Niña period (June 1998- June 1999) (see Figure 2-1 for position).

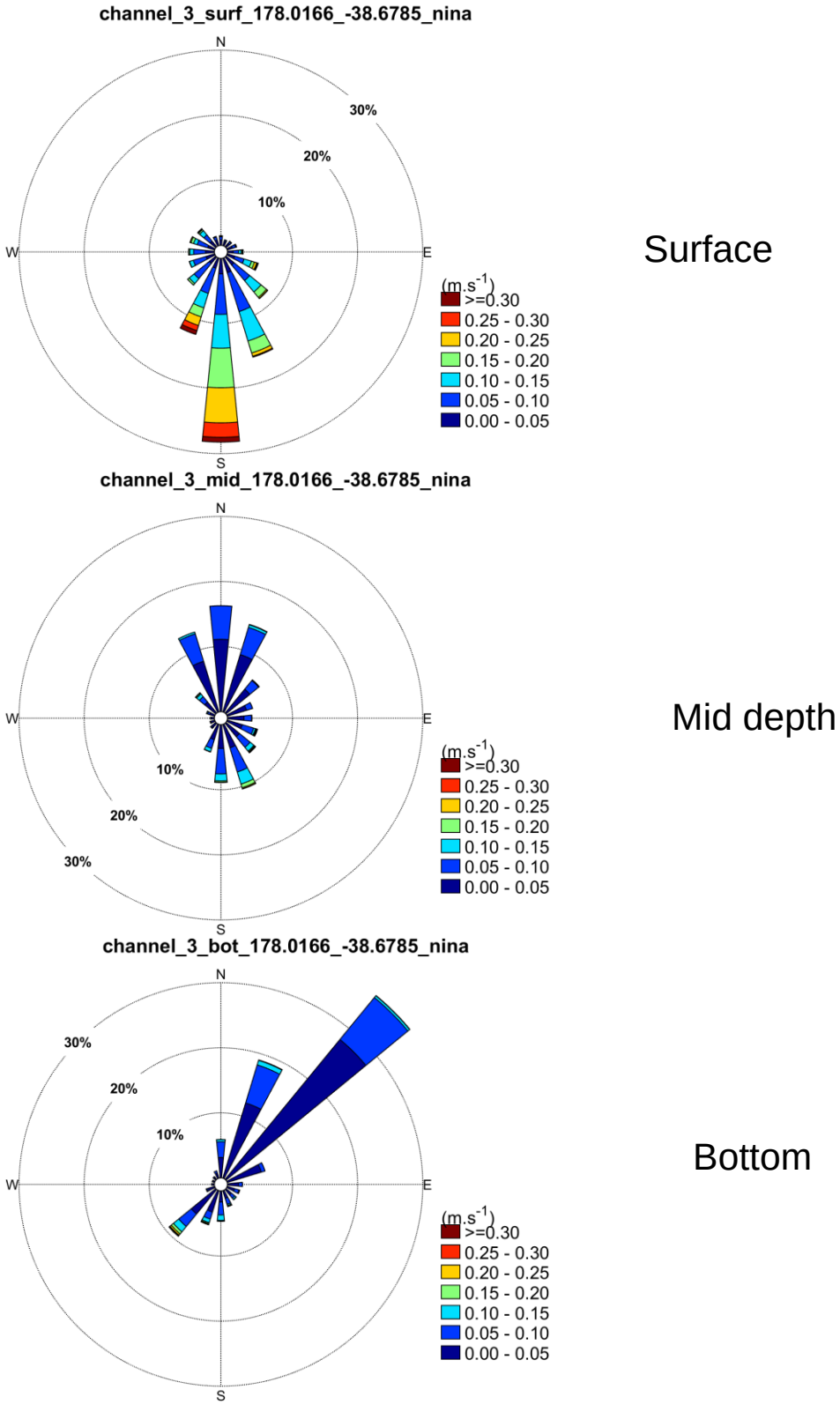

Figure 3-6 Annual current roses of surface, mid-depth, and bottom currents at site 3 for the La Niña period (June 1998- June 1999) (see Figure 2-1 for position).

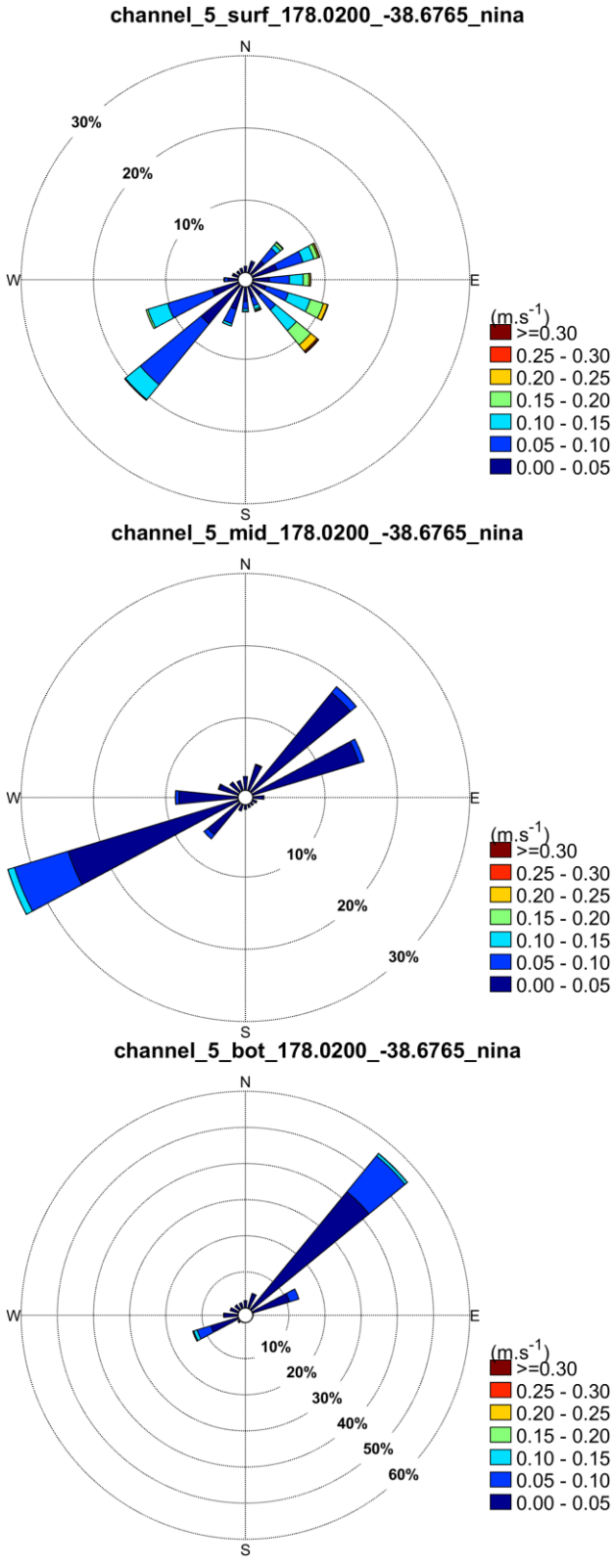

Surface

Mid depth

Bottom

Figure 3-7 Annual current roses of surface, mid-depth, and bottom currents at site 5 for the La Niña period (June 1998- June 1999) (see Figure 2-1 for position).

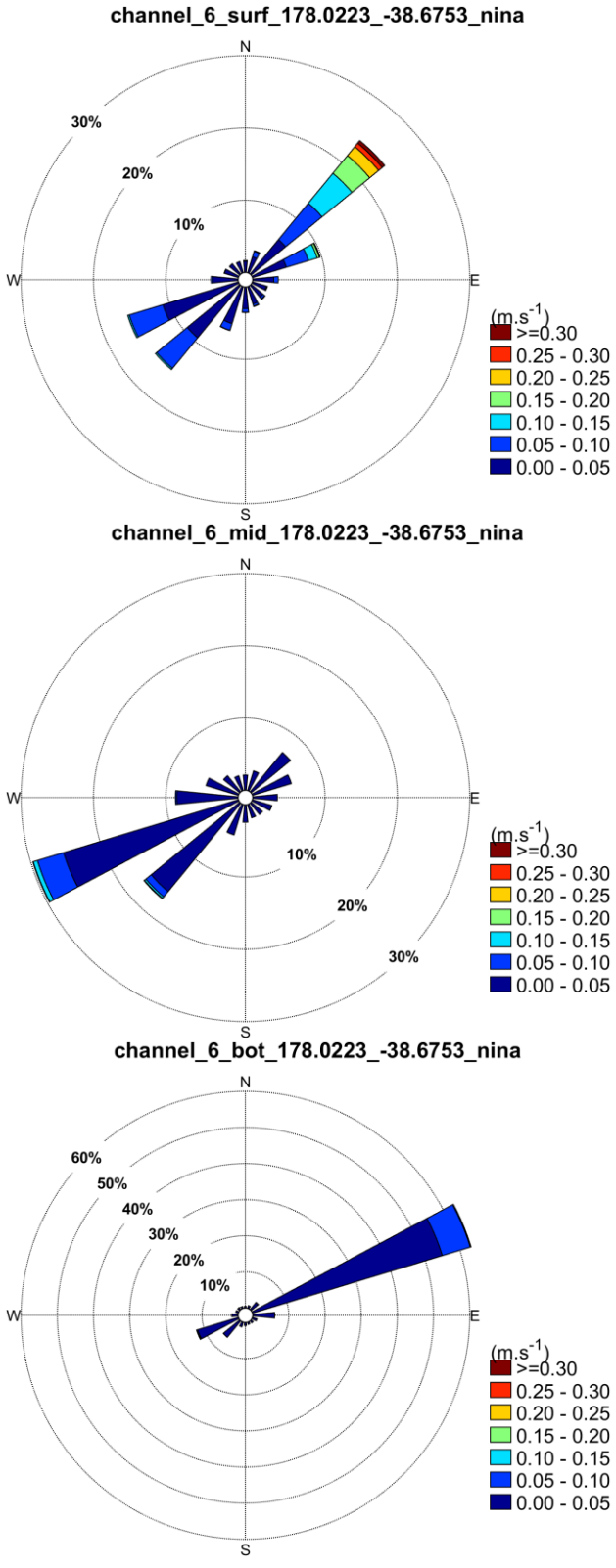

Surface

Mid depth

Bottom

Figure 3-8 Annual current roses of surface, mid-depth, and bottom currents at site 6 for the La Niña period (June 1998- June 1999) (see Figure 2-1 for position).

3.2. Probabilistic suspended sediment plumes (*ssc*) plumes and deposition

The section presents the probabilistic results derived from the entire dataset of particle trajectories predicted at each release site, throughout each annual scenario. The approach allows capturing a wide range of ambient current forcing on an annual timescale and thus provides a robust picture of the *ssc* plume footprints.

These results are presented for the different dredging operating modes considered for the channel deepening at Eastland Port Ltd, Gisborne. These include the use of the Pukunui dredger and a backhoe dredge. Details of the vessel and respective source terms used for each scenario are summarised in Table 2.5 and Table 2.7.

3.2.1. Pukunui dredger

The Pukunui dredger is currently used for the port maintenance dredging. Its hopper volume is relatively small (480 m^3) and it can operate on two modes i.e dredging only, during which sediment is sucked into the hopper, and dredging and overflow during which a dense sediment mixture is also released overboard to maximize hopper loading. The overflow is released on deck first and then reaches the oceanic environment (see Figure 3-9). The operating mode differs from the larger trailer suction hopper dredge for which the dense overflow mixture is released through a pipe, with the development of nearfield dynamics including dynamic plume descent and density current generation following seabed impact (see Figure 2-6). Instead, the overflow release is expected to be rather diffuse, and comparable to a point-source release occurring on the sea surface layer. The expected dredging cycles and associated production rates, defined from past experiences and records, were provided by the Port. The details of the cycles and sediment source terms are provided in Appendix A.

The probabilistic *ssc* plume fields expected while dredging with no overflow and assuming a settling velocity of 1 $mm.s^{-1}$ for the cohesive class, are shown in Figure 3-10 to Figure 3-13 for La Niña (June 1998-June 1999) and El Niño (June 2002-June 2003) respectively. The results for the same operating mode but assuming a settling velocity of 0.1 $mm.s^{-1}$ for the cohesive class are shown in Figure 3-14 to Figure 3-17. The probabilistic *ssc* plume fields predicted for the dredging with overflow mode are shown in Figure 3-18 to Figure 3-25.

The general plume dispersion patterns vary along the shipping channel following ambient current regimes. Dispersion pattern are typically elliptical, with an elongation northwest-southeast, at the outer channel end (Site 1). This component is conserved moving towards the Port entrance but becomes combined with an increasing northeast-southwest dispersion feature. The northeast-southwest feature is associated with the “flushing” flows in and out Port basin, constrained by the narrow Port entrance. Dispersion patterns at Site 5, located near the end of the northern jetty illustrate the transition between the outer and inner flows, with an outside northwest-southeast dispersion and inside northeast-southwest dispersion components. Dispersion patterns at the inner port sites are expectedly elongated in the northeast-southwest direction, following the general channel orientation.

Modulations of the dispersion patterns with respect to the La Niña / El Niño periods are limited, with most evident variations are visible on the outer sites. The consistent patterns despite the different climate contexts are not surprising given the position of the Port, situated well inside the Bay, and thus less exposed to modulations in larger scale hydrodynamics.

Plume dispersion simulations were reproduced assuming two different settling velocities for the cohesive sediment class, to address uncertainties on the effective settling velocities of flocculated material which are difficult to estimate in absence of comprehensive *in-situ* data. Longer settling times allow sediment to be transported over longer distances and thus generate larger dispersion footprints, however this is also associated with a relatively increased dilution compared to faster settling sediment. It is noted that although some of the dispersion footprints associated with the smaller settling velocity (0.1 $mm.s^{-1}$) may seem significant, footprint "edges" are often associated with *ssc* levels of order 1-10 $mg.L^{-1}$ which can be smaller than the background *ssc* (e.g. due to river discharges or other sources).

Overall, the use of an overflow phase in addition to the continuous seabed dredging results in the most significant increase of predicted *ssc* levels, throughout the entire water column. This can be directly attributed to the large quantities of sediment released in the environment as well as the effective release "mode" i.e. sediment released at the surface (as used for Pukunui) or de-entrained from descending dynamic-plume throughout the entire water column (larger TSHD vessels). Here, it is noted that the effective *ssc* increase could be mitigated by altering the operating mode (no overflow or use a "green valve") and/or duration of the overflow phase.

As outlined in section 2.3.3, the simulations have assumed static sediment release at each site along the channel (Figure 2-1) and results should therefore be interpreted as worst-case plume footprints in terms extents and suspended sediment concentration levels which are useful metrics for impact assessments.

In reality, a moving dredger will allow some dilution of the *ssc* plumes as it navigates, particularly in the outer channel region where distances covered over an infilling cycle may be important. To provide a basis for comparison with the static results, a scenario reproducing a dredger moving along the outer channel was simulated, over a 7 day period (Dec. 1998). Over that period, the dredger is assumed to be dredging (i.e. releasing sediment) while moving from site 1 to 5, and back, over a 2 hour period (including 30 min dredging only followed by 1h30 of dredging and overflowing), then stop for 2 hours i.e. travelling to disposal site. This is reproduced continuously over the 7-day period.

The resulting mean *ssc* plumes are shown in Figure 3-26 for assuming settling velocities of 1.0 and 0.1 $mm.s^{-1}$ for the cohesive class. The *ssc* plumes are indeed clearly elongated along the shipping channel and *ssc* magnitudes are smaller than those predicted for the static cases (e.g. see Figure 3-18). This can be directly attributed to the increased dilution potential associated with the dredger forward motion which therefore releases sediment at different positions over time, thus spreading the sediment load.

Figure 3-9 Pukunui vessel releasing its overflow mixture in the oceanic environment. Note the overflow mixture is initially released over the deck, and then flows overboard, which reduces its initial downward momentum and limits the formation of a dynamic plume phase (Figure 2-5).

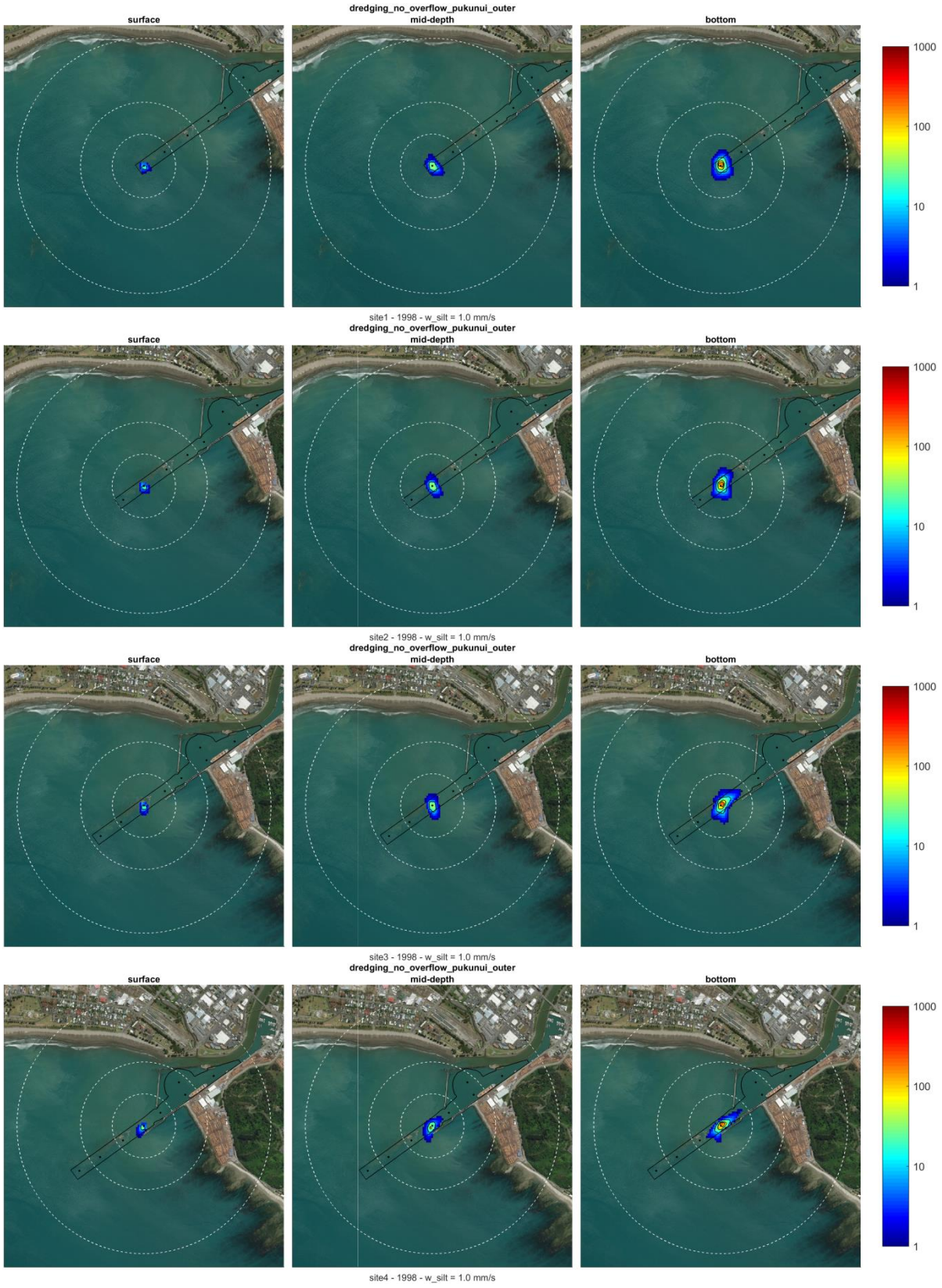

Figure 3-10 Probabilistic *ssc* fields [mg.L^{-1}] while dredging **with no overflow**, in the outer channel (sites 1-4), using the Pukunui vessel (V=480 m^3), derived from the annual La Niña period (June 1998-June 1999). The results assumed a settling velocity of 1 mm.s^{-1} for the cohesive sediment class. Dashed white circles have radiuses of 250, 500 and 1000 m. The 10, 50 and 100 mg.L^{-1} contours are shown in black.

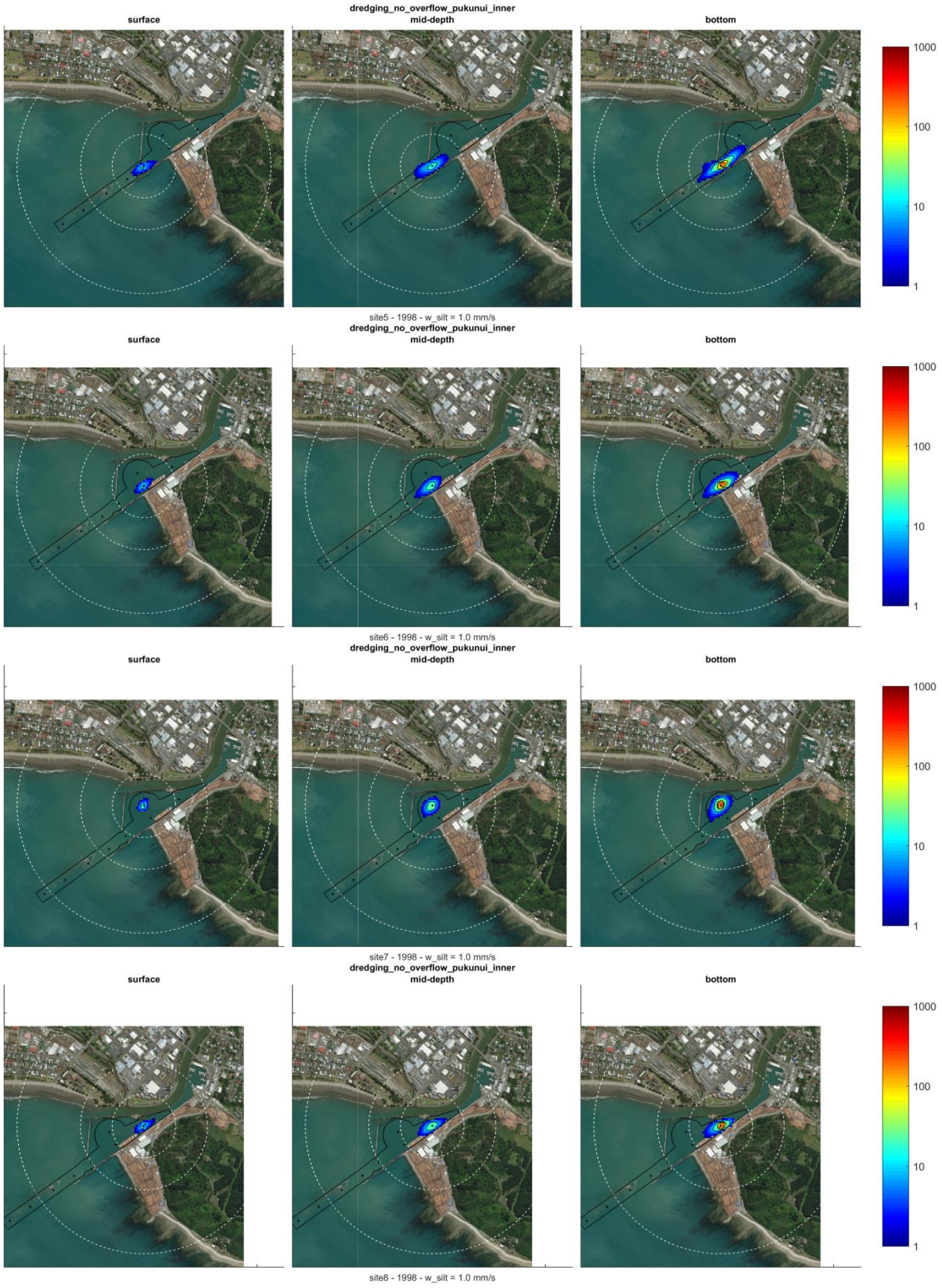

Figure 3-11 Probabilistic ssc fields [mg.L-1] while dredging with no overflow, in the inner channel (sites 5-8), using the Pukunui vessel (V=480 m3), derived from the annual La Niña period (June 1998-June 1999). The results assumed a settling velocity of 1 mm.s-1 for the cohesive sediment class. Dashed white circles have radiuses of 250, 500 and 1000 m. The 10, 50 and 100 mg.L-1 contours are shown in black.

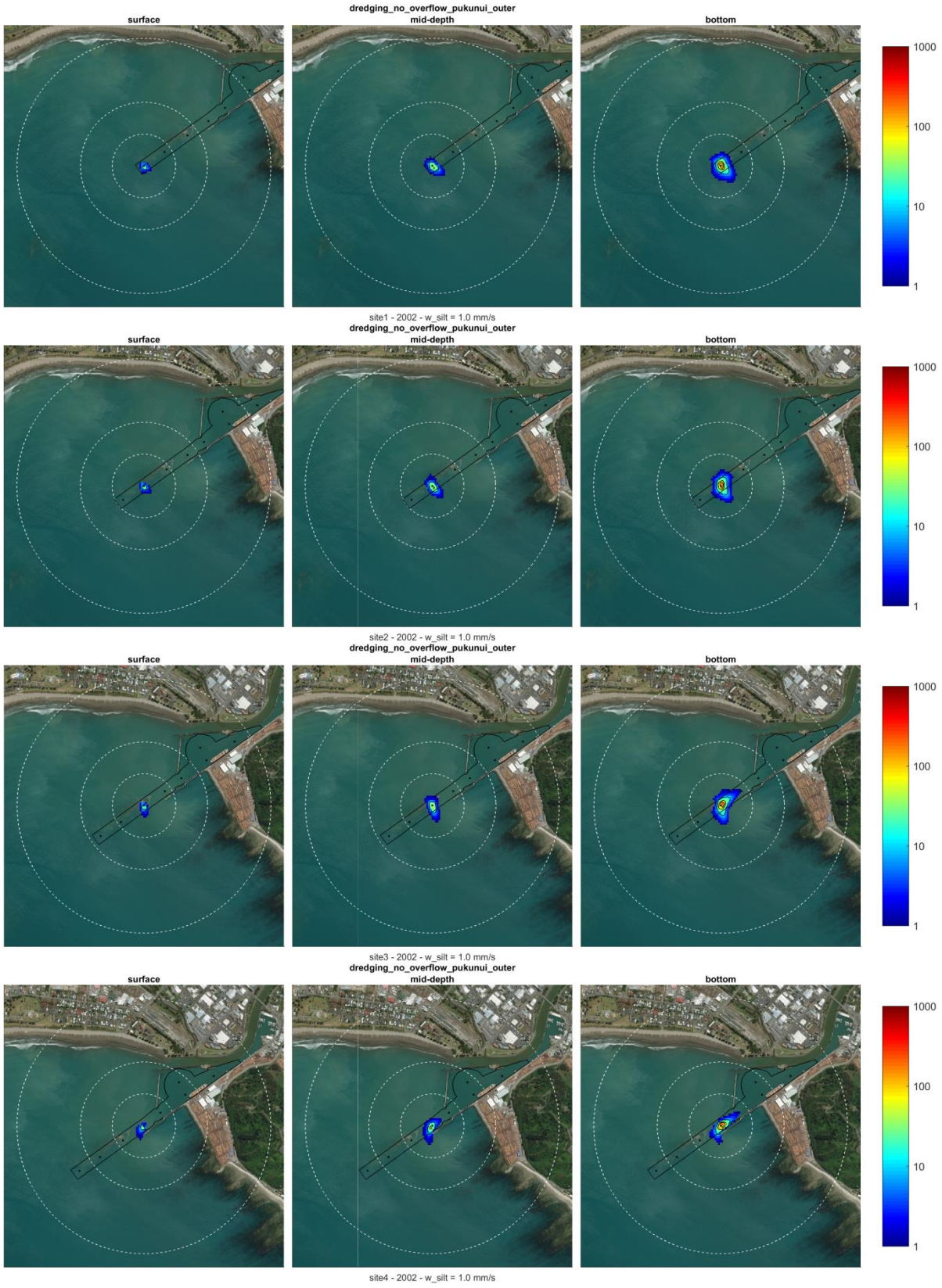

Figure 3-12 Probabilistic *ssc* fields [mg.L^{-1}] while dredging **with no overflow**, in the outer channel (sites 1-4), using the Pukunui vessel (V=480 m^3), derived from the annual El Niño period (June 2002-June 2003). The results assumed a settling velocity of 1 mm.s^{-1} for the cohesive sediment class. Dashed white circles have radiuses of 250, 500 and 1000 m. The 10, 50 and 100 mg.L^{-1} contours are shown in black.

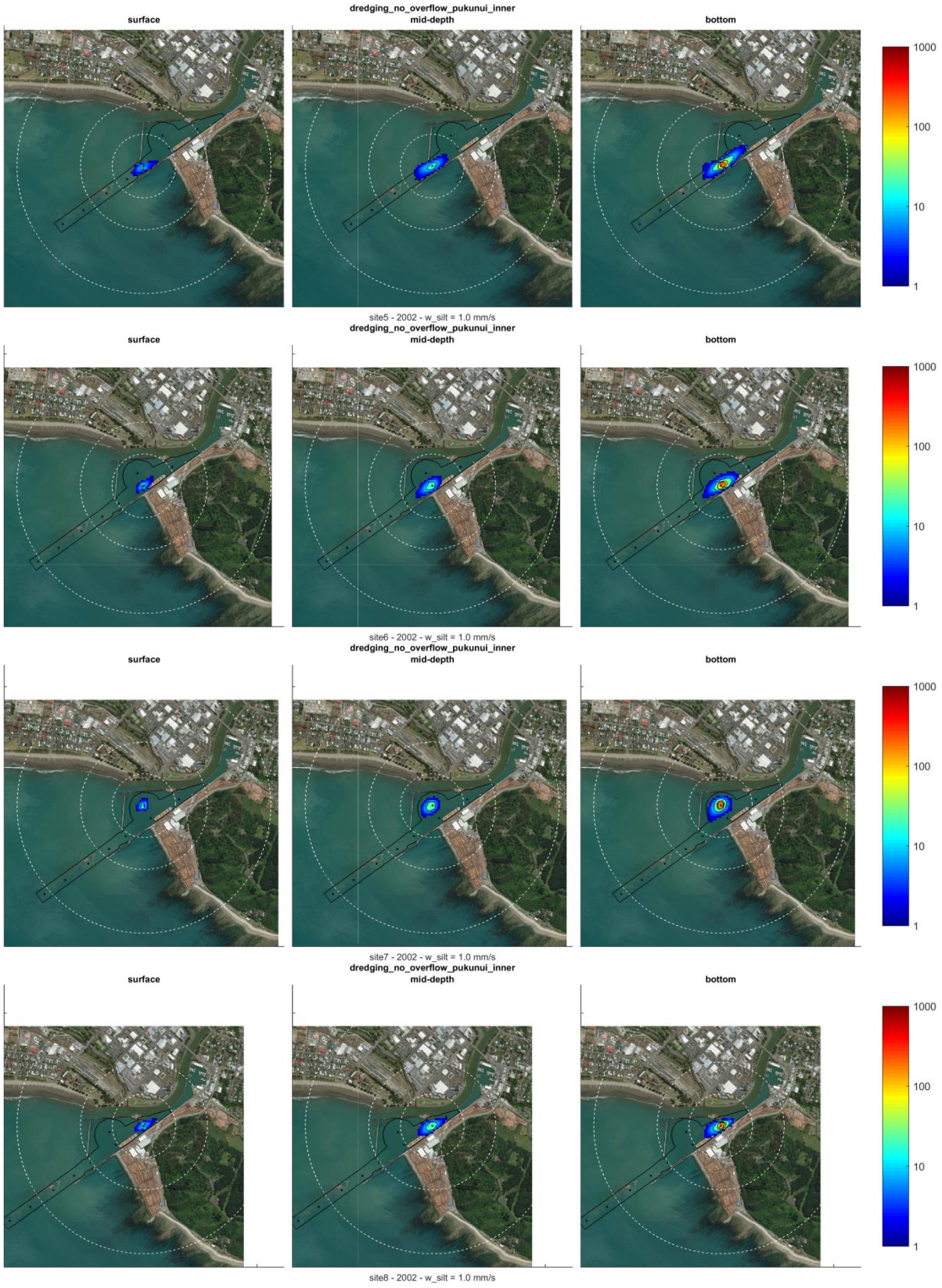

Figure 3-13 Probabilistic *ssc* fields [mg.L^{-1}] while dredging **with no overflow**, in the inner channel (sites 5-8), using the Pukunui vessel (V=480 m^3), derived from the annual El Niño period (June 2002-June 2003). The results assumed a settling velocity of 1 mm.s^{-1} for the cohesive sediment class. Dashed white circles have radiuses of 250, 500 and 1000 m. The 10, 50 and 100 mg.L^{-1} contours are shown in black.

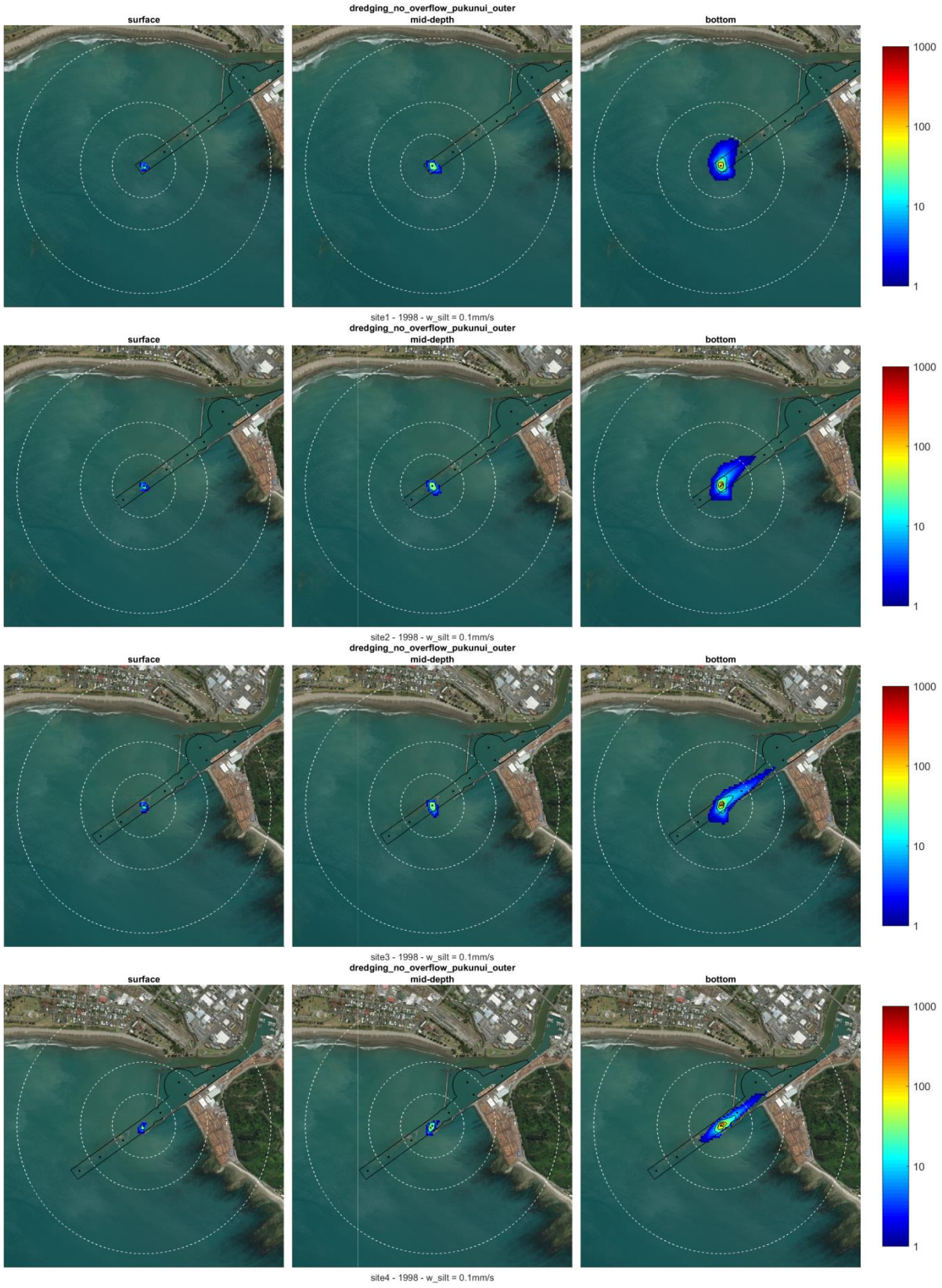

Figure 3-14 Probabilistic *ssc* fields [mg.L^{-1}] while dredging **with no overflow**, in the outer channel (sites 1-4), using the Pukunui vessel (V=480 m^3), derived from the annual La Niña period (June 1998-June 1999). The results assumed a settling velocity of 0.1 mm.s^{-1} for the cohesive sediment class. Dashed white circles have radiuses of 250, 500 and 1000 m. The 10, 50 and 100 mg.L^{-1} contours are shown in black.

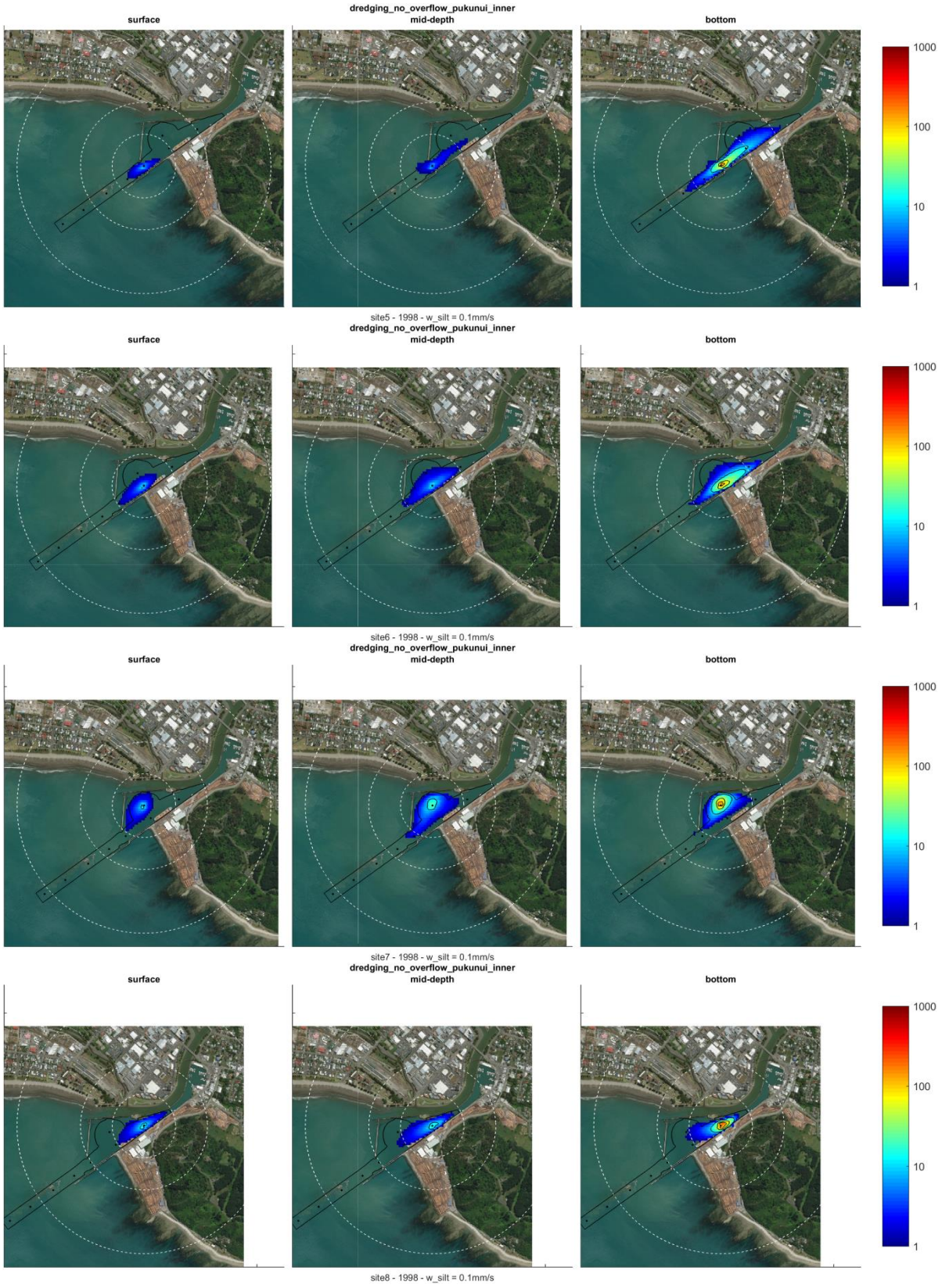

Figure 3-15 Probabilistic *ssc* fields [mg.L^{-1}] while dredging **with no overflow**, in the inner channel (sites 5-8), using the Pukunui vessel (V=480 m^3), derived from the annual La Niña period (June 1998-June 1999). The results assumed a settling velocity of 0.1 mm.s^{-1} for the cohesive sediment class. Dashed white circles have radiuses of 250, 500 and 1000 m. The 10, 50 and 100 mg.L^{-1} contours are shown in black.

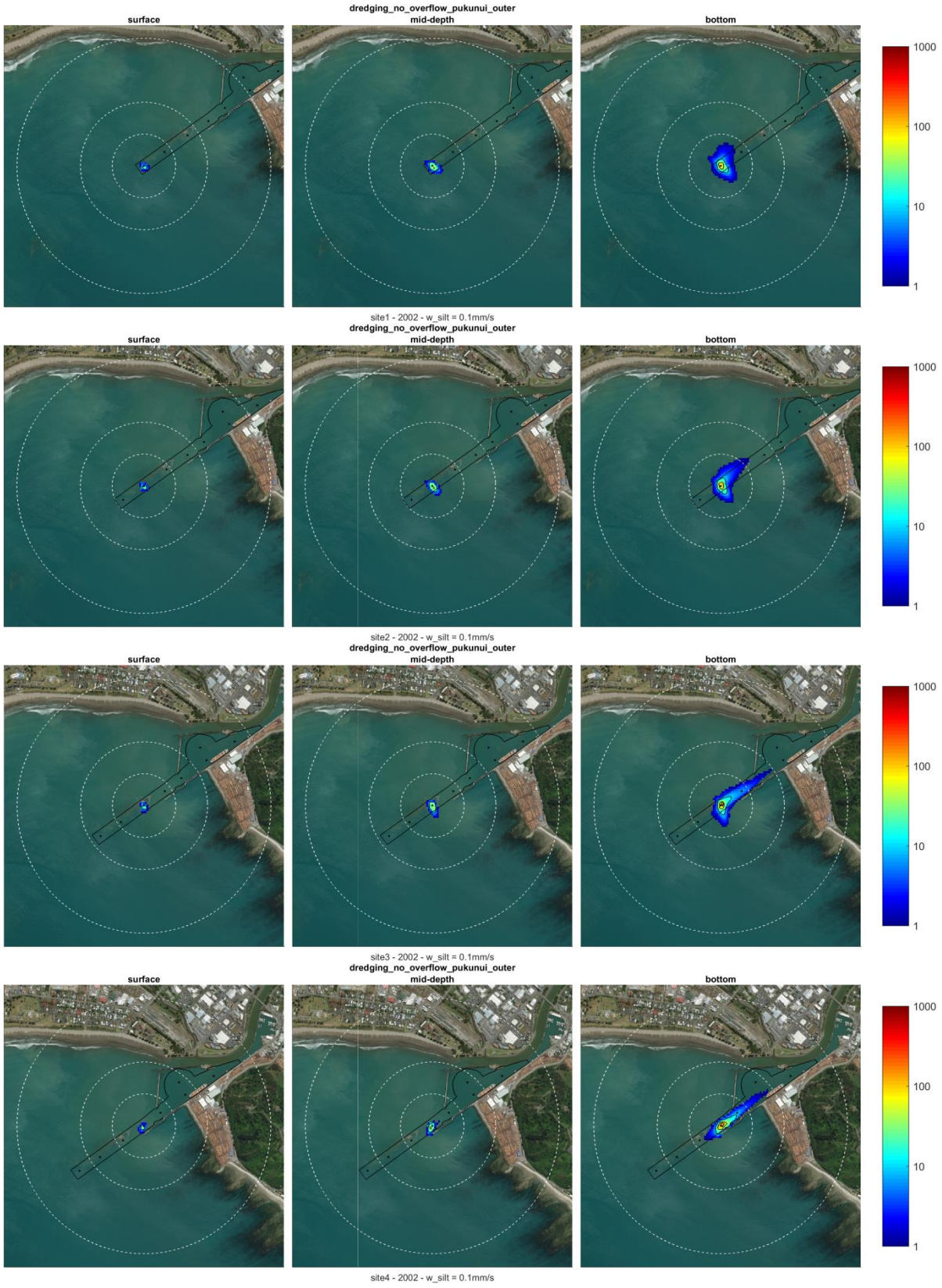

Figure 3-16 Probabilistic *ssc* fields [mg.L^{-1}] while dredging **with no overflow**, in the outer channel (sites 1-4), using the Pukunui vessel (V=480 m^3), derived from the annual El Niño period (June 2002-June 2003). The results assumed a settling velocity of 0.1 mm.s^{-1} for the cohesive sediment class. Dashed white circles have radiuses of 250, 500 and 1000 m. The 10, 50 and 100 mg.L^{-1} contours are shown in black.

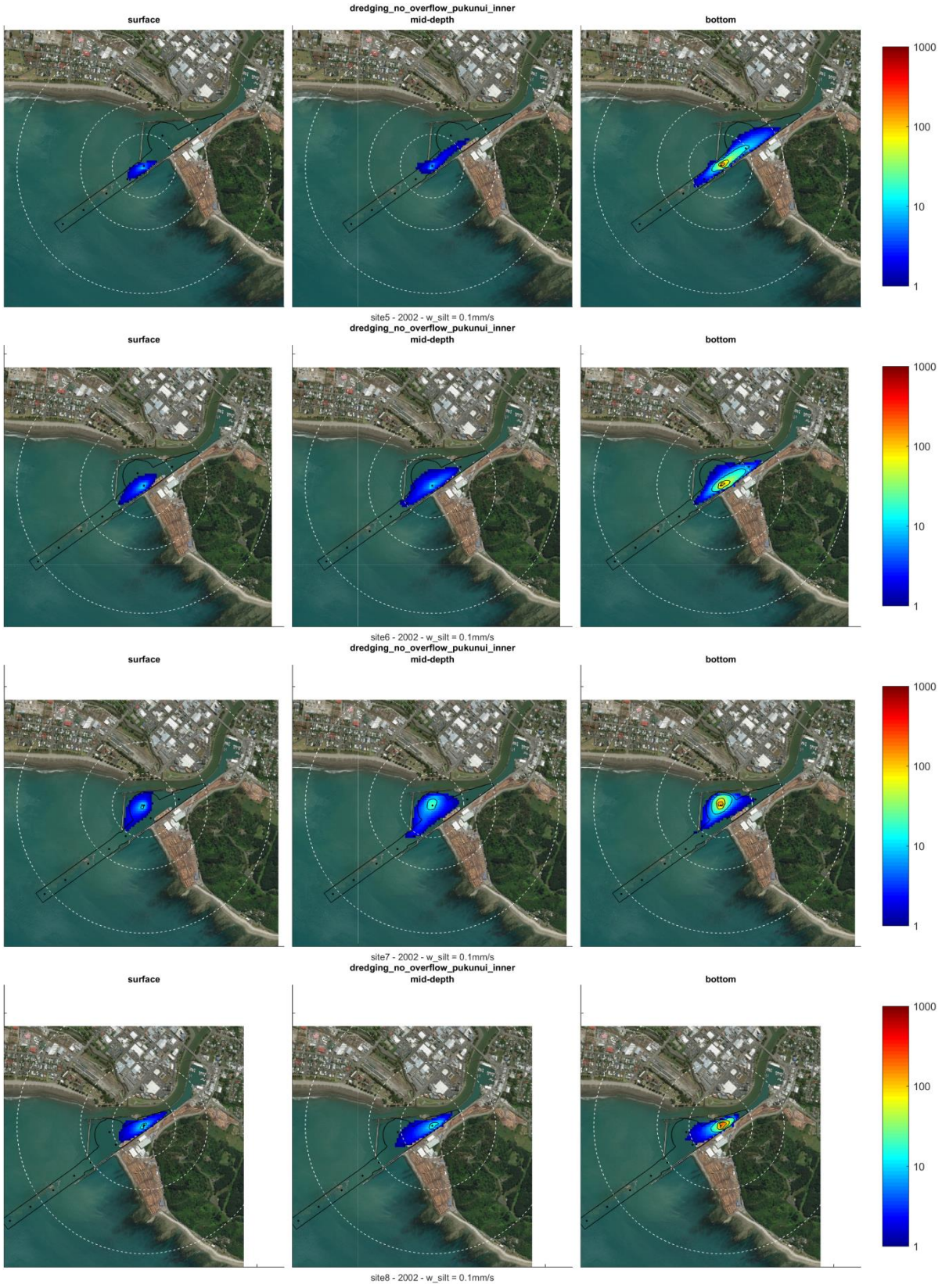

Figure 3-17 Probabilistic *ssc* fields [mg.L^{-1}] while dredging **with no overflow**, in the inner channel (sites 5-8), using the Pukunui vessel (V=480 m^3), derived from the annual El Niño period (June 2002-June 2003). The results assumed a settling velocity of 0.1 mm.s^{-1} for the cohesive sediment class. Dashed white circles have radiuses of 250, 500 and 1000 m. The 10, 50 and 100 mg.L^{-1} contours are shown in black.

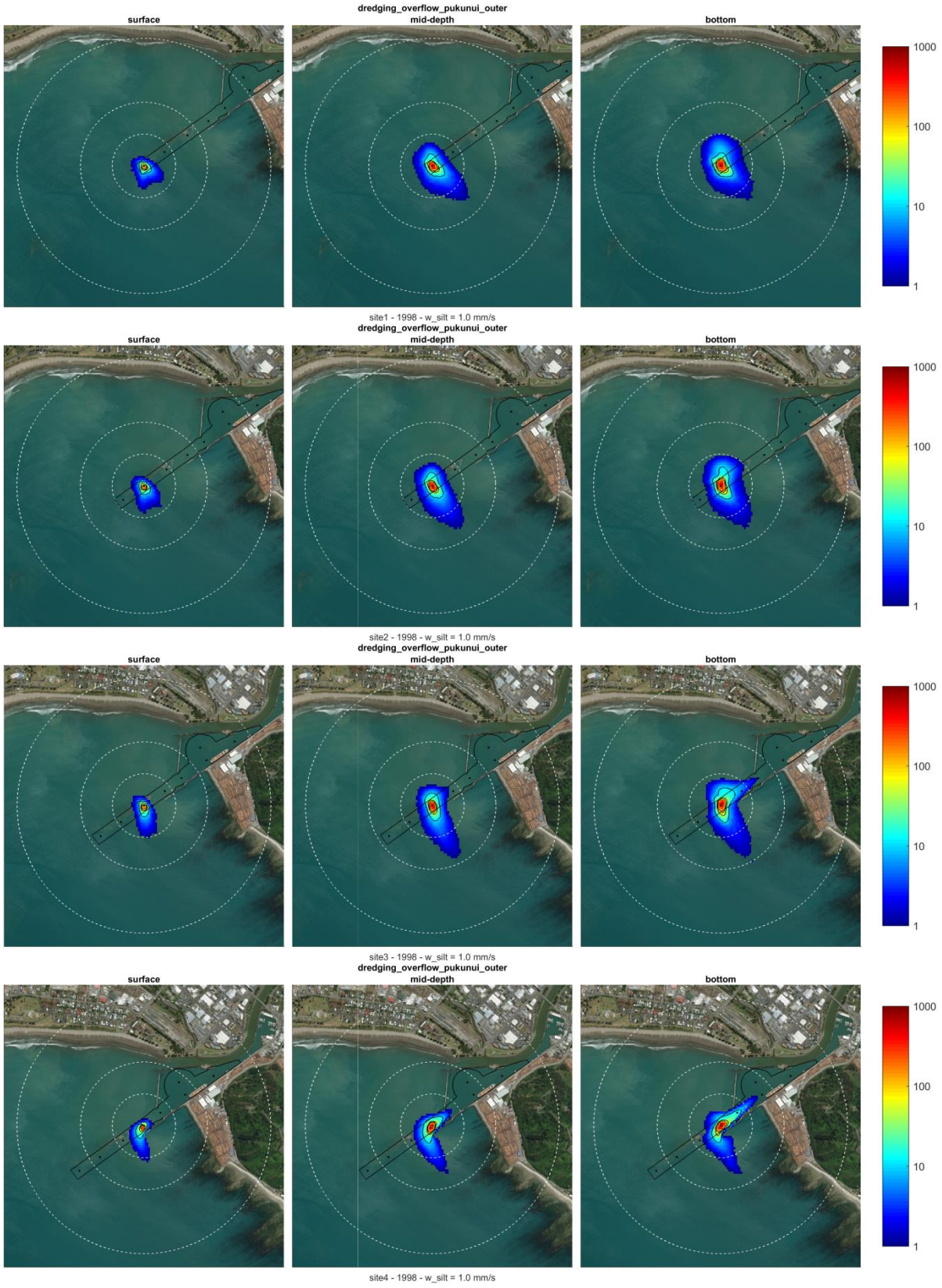

Figure 3-18 Probabilistic *ssc* fields [mg.L^{-1}] while dredging **with overflow**, in the outer channel (sites 1-4), using the Pukunui vessel (V=480 m^3), derived from the annual La Niña period (June 1998-June 1999). The results assumed a settling velocity of 1 mm.s^{-1} for the cohesive sediment class. Dashed white circles have radiuses of 250, 500 and 1000 m. The 10, 50 and 100 mg.L^{-1} contours are shown in black.

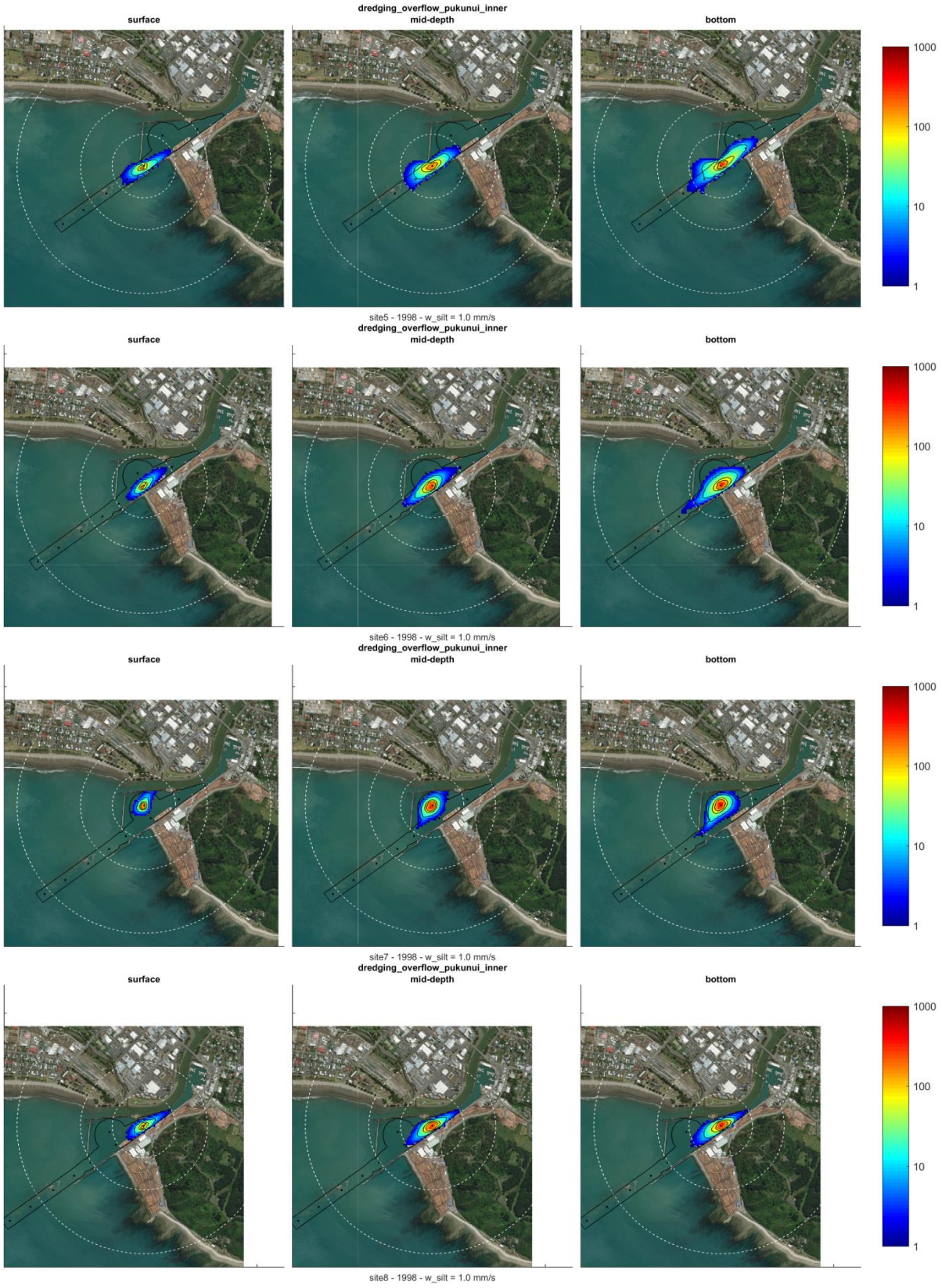

Figure 3-19 Probabilistic *ssc* fields [mg.L^{-1}] while dredging **with overflow**, in the inner channel (sites 5-8), using the Pukunui vessel (V=480 m^3), derived from the annual La Niña period (June 1998-June 1999). The results assumed a settling velocity of 1 mm.s^{-1} for the cohesive sediment class. Dashed white circles have radiuses of 250, 500 and 1000 m. The 10, 50 and 100 mg.L^{-1} contours are shown in black.

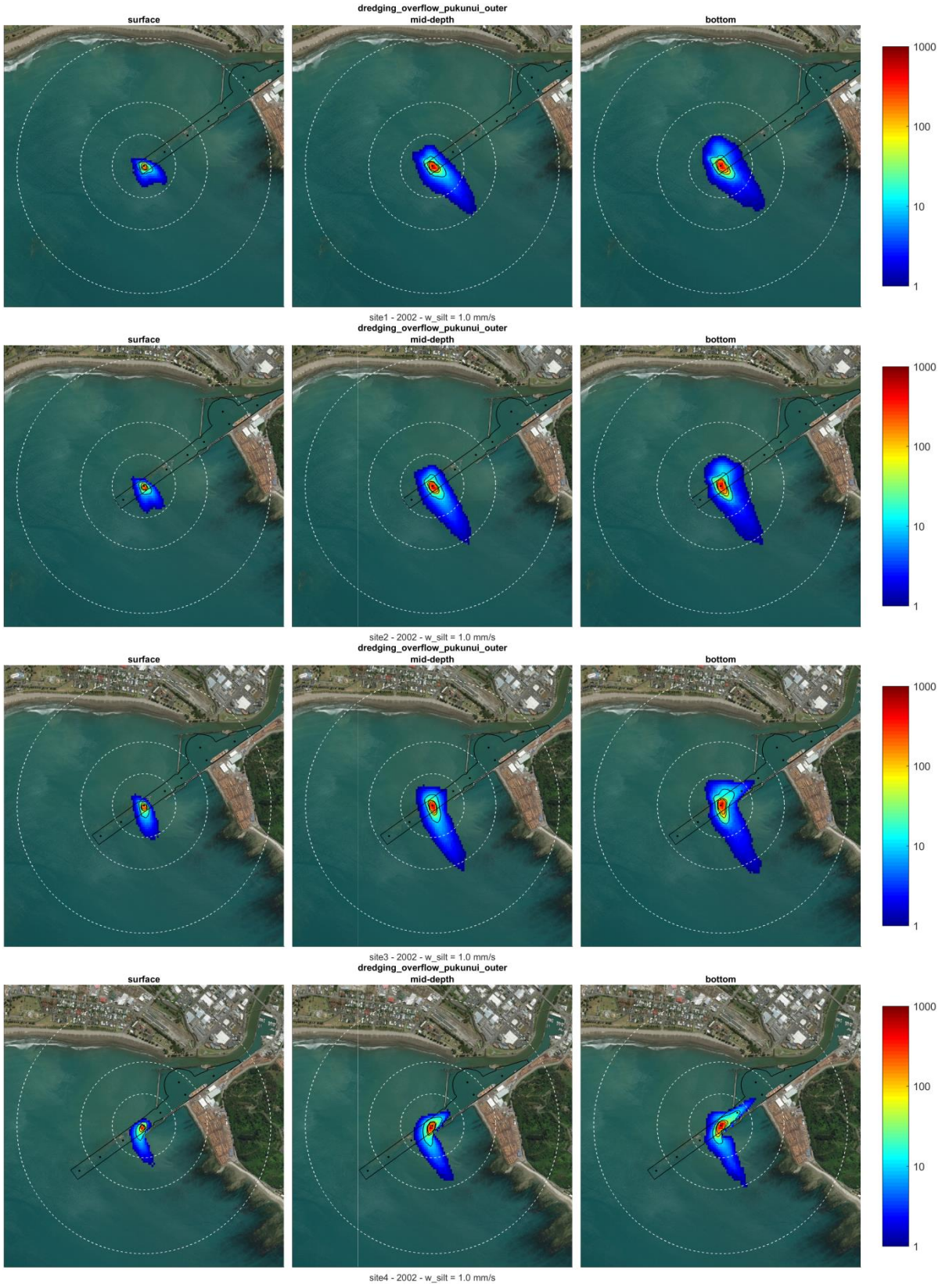

Figure 3-20 Probabilistic *ssc* fields [mg.L^{-1}] while dredging **with overflow**, in the outer channel (sites 1-4), using the Pukunui vessel (V=480 m^3), derived from the annual El Niño period (June 2002-June 2003). The results assumed a settling velocity of 1.0 mm.s^{-1} for the cohesive sediment class. Dashed white circles have radiuses of 250, 500 and 1000 m. The 10, 50 and 100 mg.L^{-1} contours are shown in black.

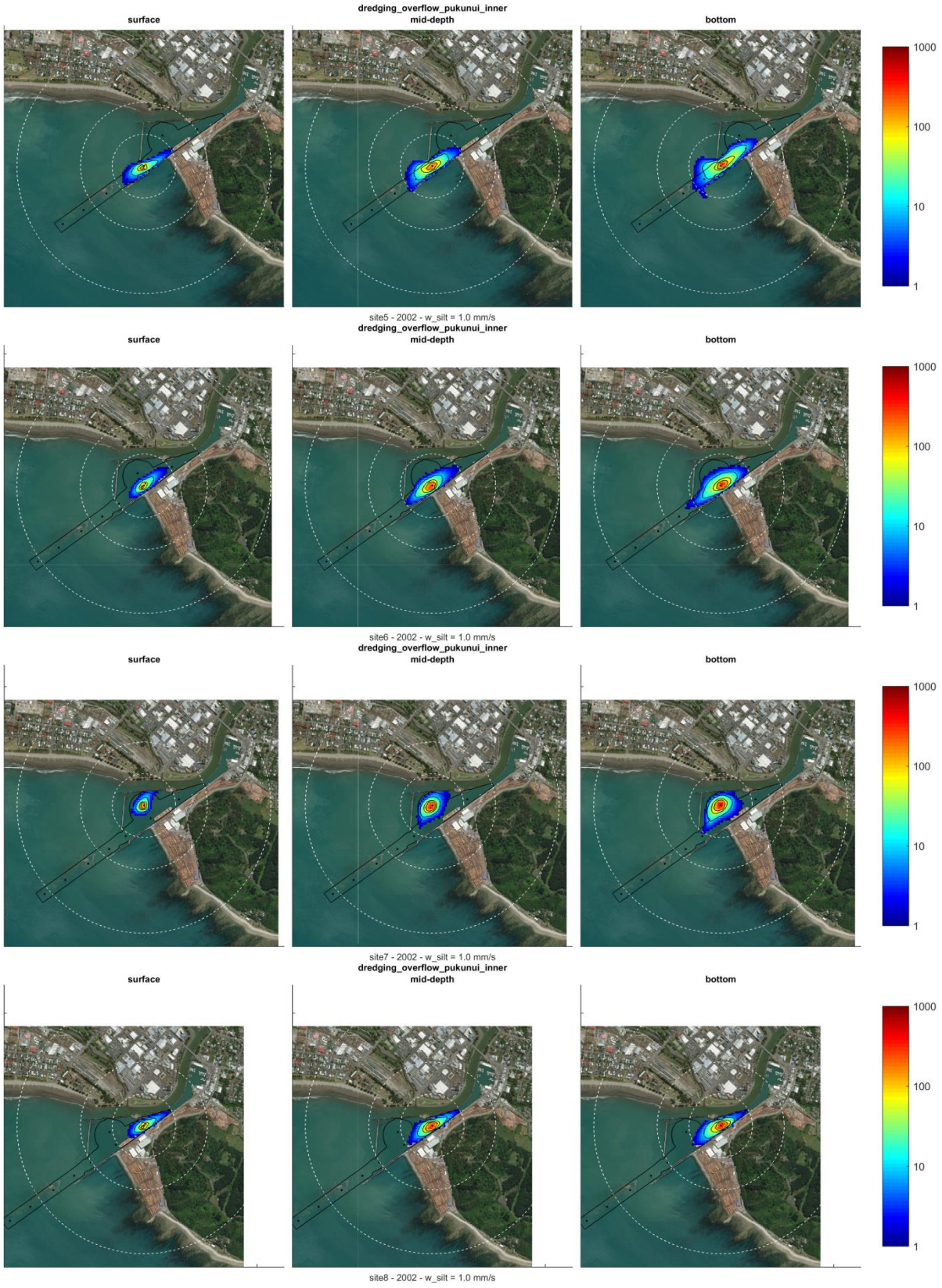

Figure 3-21 Probabilistic *ssc* fields [mg.L^{-1}] while dredging **with overflow**, in the inner channel (sites 5-8), using the Pukunui vessel (V=480 m^3), derived from the annual El Niño period (June 2002-June 2003). The results assumed a settling velocity of 1.0 mm.s^{-1} for the cohesive sediment class. Dashed white circles have radiuses of 250, 500 and 1000 m. The 10, 50 and 100 mg.L^{-1} contours are shown in black.

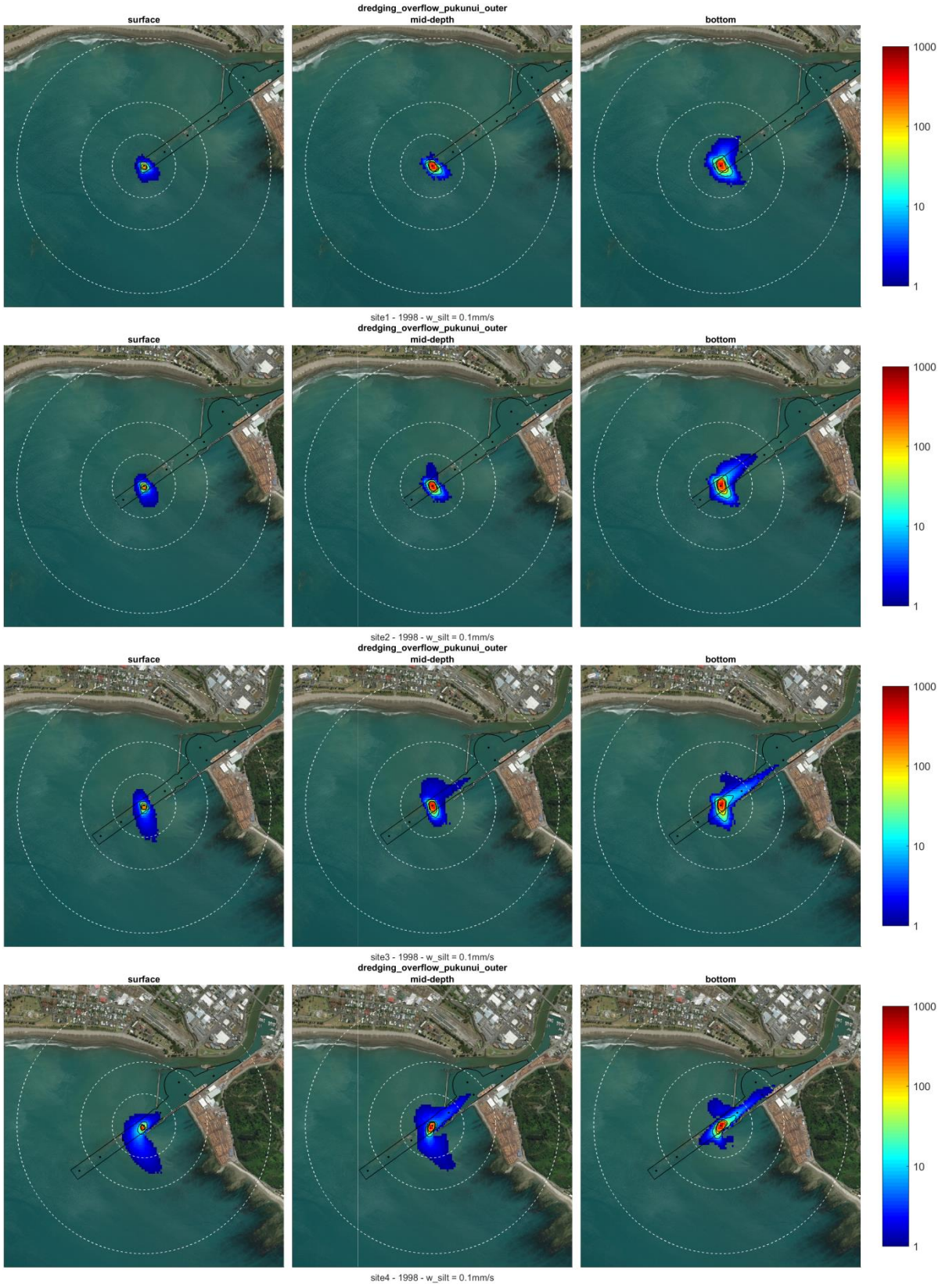

Figure 3-22 Probabilistic *ssc* fields [mg.L^{-1}] while dredging **with overflow**, in the outer channel (sites 1-4), using the Pukunui vessel (V=480 m^3), derived from the annual La Niña period (June 1998-June 1999). The results assumed a settling velocity of 0.1 mm.s^{-1} for the cohesive sediment class. Dashed white circles have radiuses of 250, 500 and 1000 m. The 10, 50 and 100 mg.L^{-1} contours are shown in black.

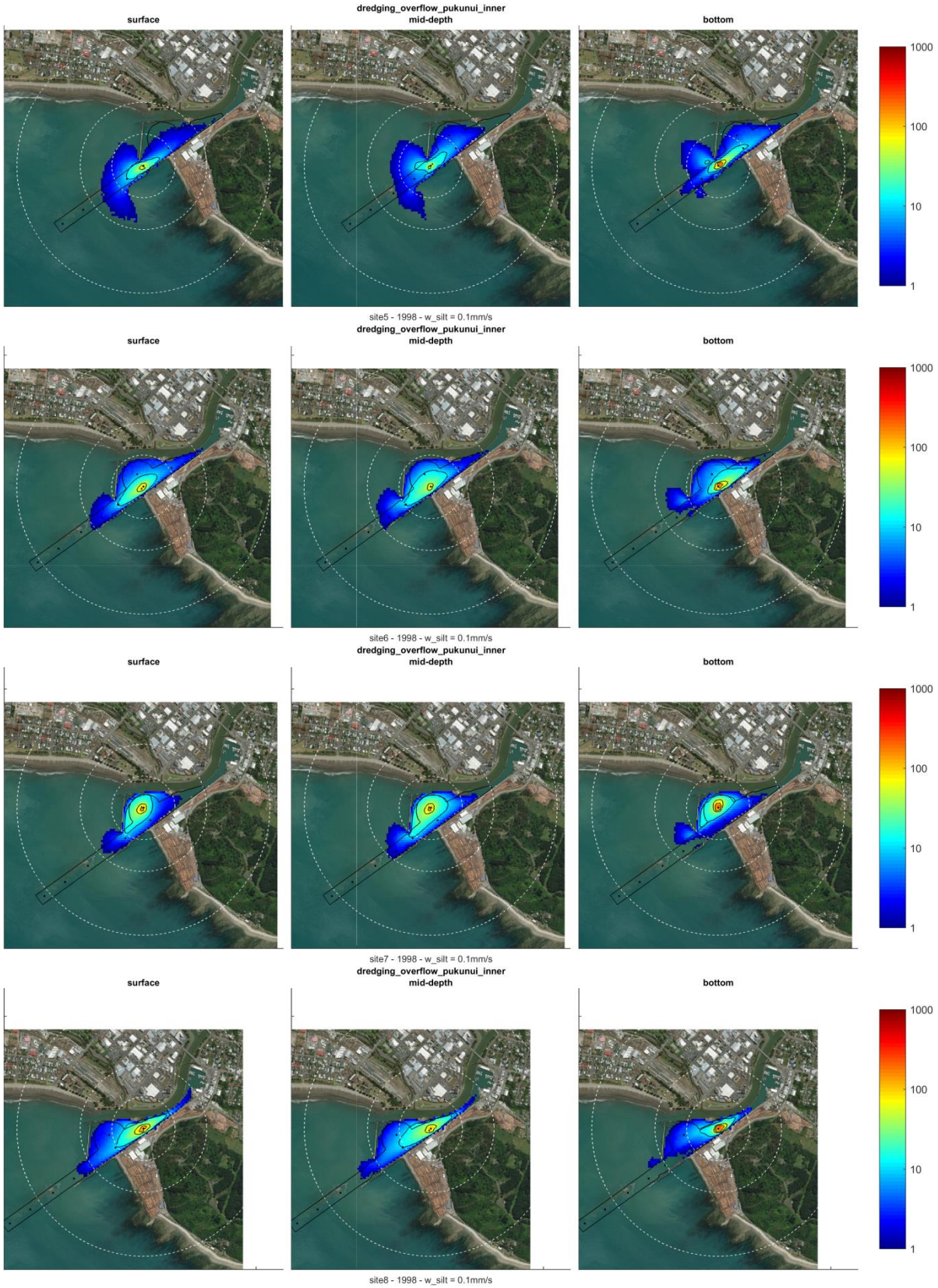

Figure 3-23 Probabilistic *ssc* fields [mg.L^{-1}] while dredging **with overflow**, in the inner channel (sites 5-8), using the Pukunui vessel (V=480 m^3), derived from the annual La Niña period (June 1998-June 1999). The results assumed a settling velocity of 0.1 mm.s^{-1} for the cohesive sediment class. Dashed white circles have radiuses of 250, 500 and 1000 m. The 10, 50 and 100 mg.L^{-1} contours are shown in black.

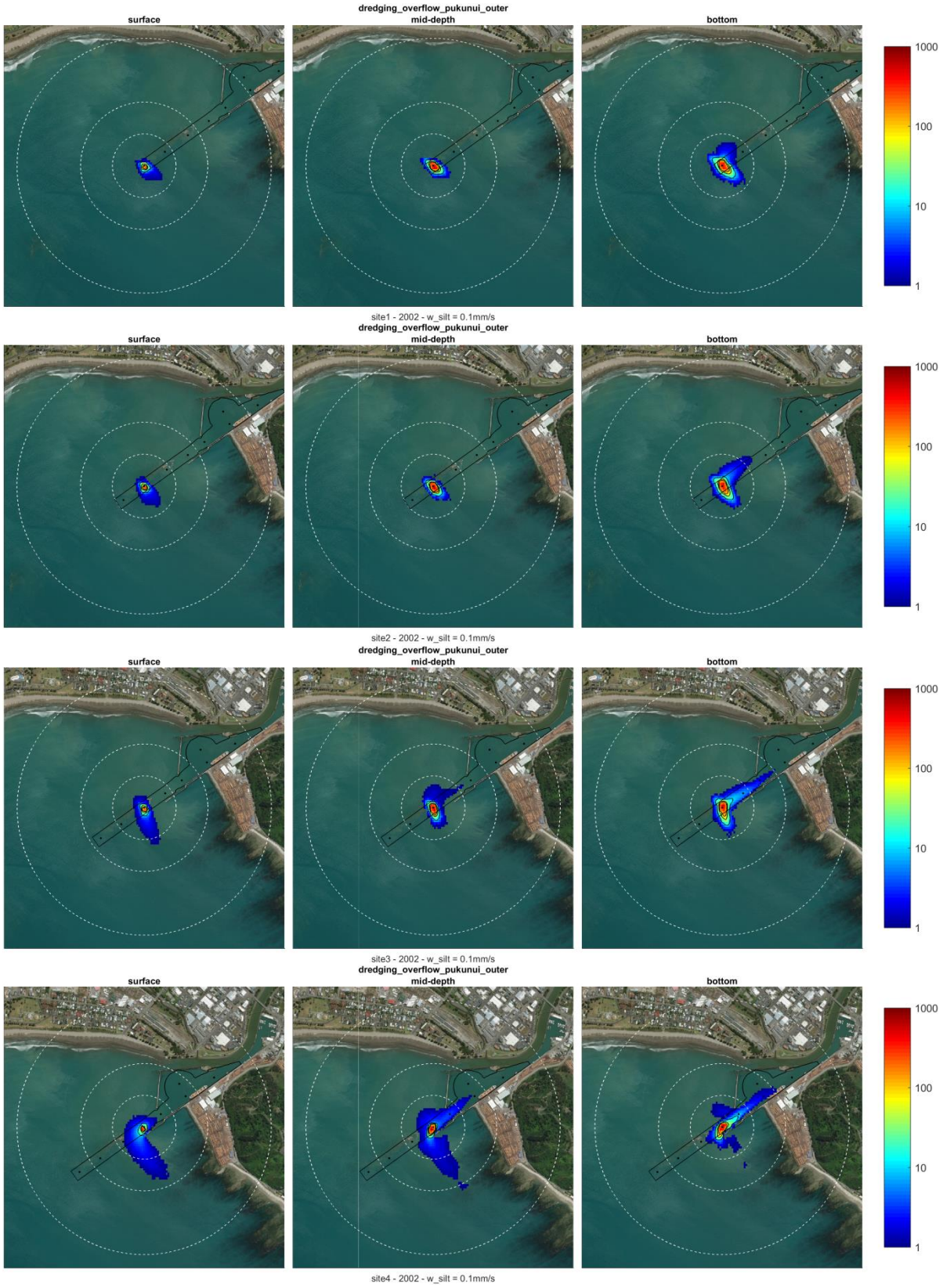

Figure 3-24 Probabilistic *ssc* fields [mg.L^{-1}] while dredging **with overflow**, in the outer channel (sites 1-4), using the Pukunui vessel (V=480 m^3), derived from the annual El Niño period (June 2002-June 2003). The results assumed a settling velocity of 0.1 mm.s^{-1} for the cohesive sediment class. Dashed white circles have radiuses of 250, 500 and 1000 m. The 10, 50 and 100 mg.L^{-1} contours are shown in black.

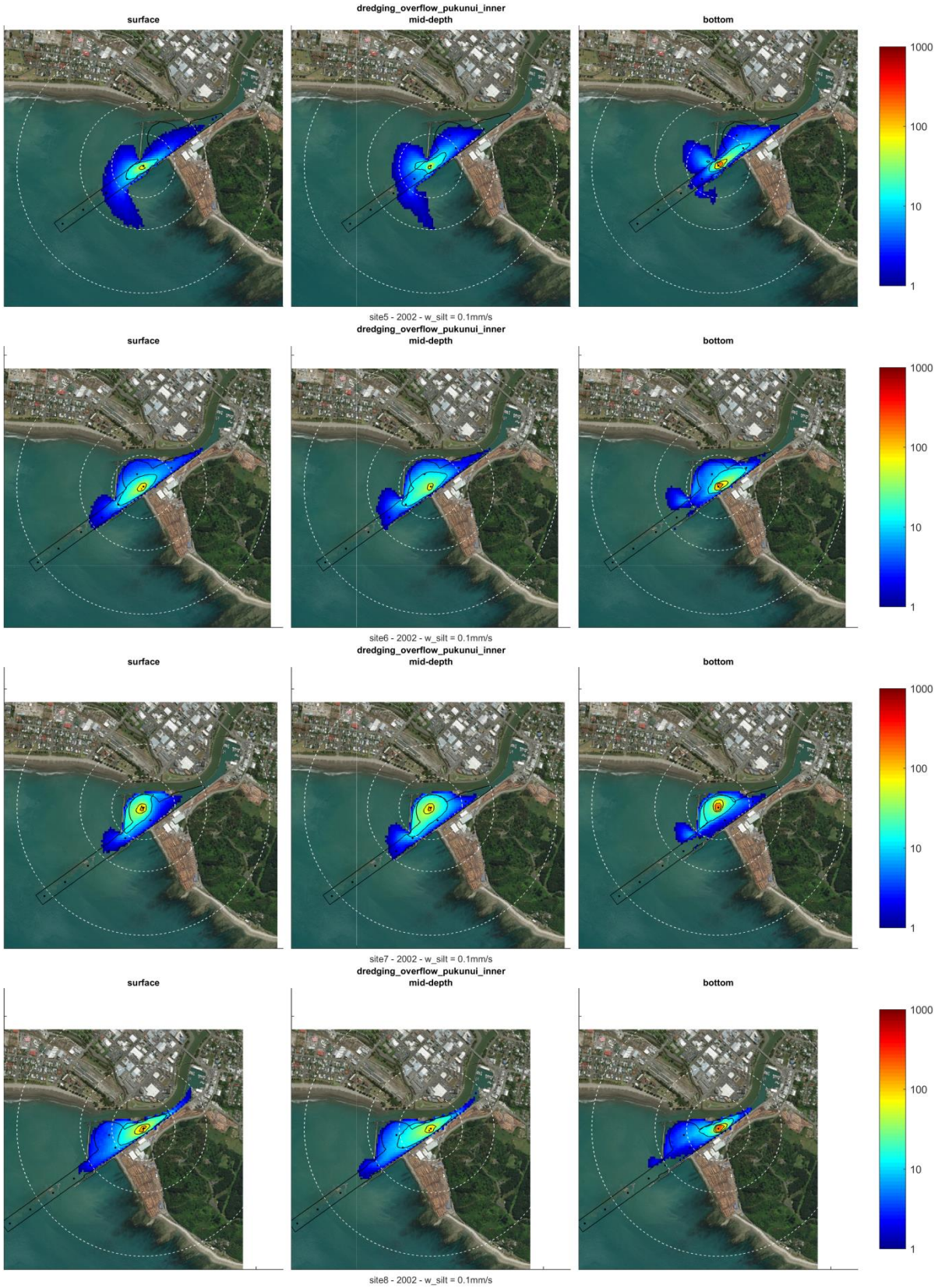

Figure 3-25 Probabilistic *ssc* fields [mg.L^{-1}] while dredging **with overflow**, in the inner channel (sites 5-8), using the Pukunui vessel (V=480 m^3), derived from the annual El Niño period (June 2002-June 2003). The results assumed a settling velocity of 0.1 mm.s^{-1} for the cohesive sediment class. Dashed white circles have radiuses of 250, 500 and 1000 m. The 10, 50 and 100 mg.L^{-1} contours are shown in black.

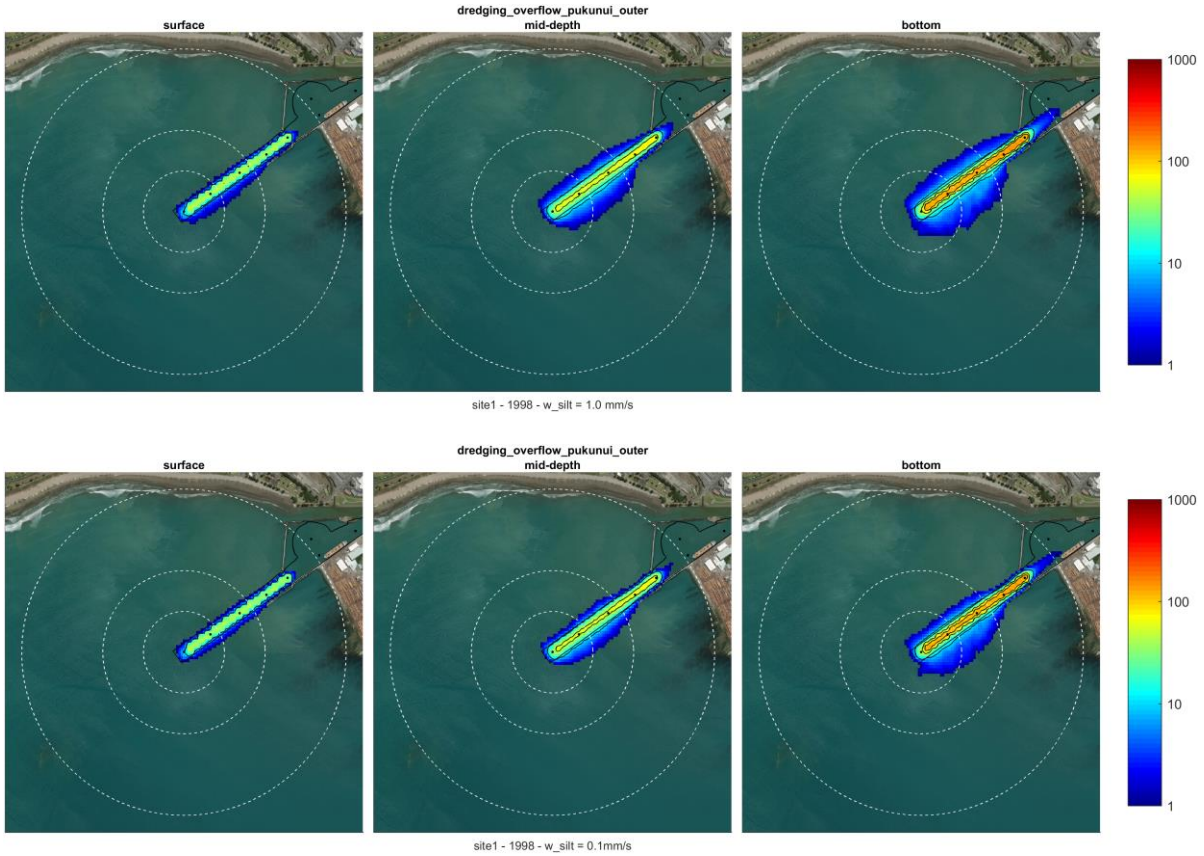

Figure 3-26 Mean *ssc* fields while **dredging with overflow**, in the outer channel region (sites 1-5), using the Pukunui vessel (V=480 m^3). The *ssc* fields are derived from a 7 day simulation during which the dredger is assumed to be dredging (i.e. releasing sediment) while moving from site 1 to 5, and back, over a 2 hour period (including 30 min dredging only then 1h30 of dredging and overflowing), then stop for 2 hours i.e. travelling to disposal site. Results assuming settling velocities of 1.0 and 0.1 $mm.s^{-1}$ for the cohesive sediment class are shown in the top and bottom panels respectively. Dashed white circles have radiuses of 250, 500 and 1000 m. The 10, 50 and 100 $mg.L^{-1}$ contours are shown in black.

3.2.2. Backhoe dredger

Backhoe dredging may be used in areas that cannot be easily accessed by the Pukunui vessel, such as the close vicinity of the berths. This operating mode consists in a backhoe, placed onto a barge, removing sediment from the seabed with a bucket, and then placing it into the Pukunui hopper. Assuming a hopper filling ratio similar to what is achieved during normal dredging conditions (~220 m^3 of sediment removed per cycle), and video footage of backhoe operations (Figure 3-27), a generic infilling time of 4 hours was assumed in order to define the source terms (see Appendix A for details).

The probabilistic *ssc* plume fields expected while dredging with a backhoe and assuming a settling velocity of 1 $mm.s^{-1}$ for the cohesive class, are shown in Figure 3-28 and Figure 3-29 for La Niña (June 1998-June 1999) and El Niño (June 2002-June 2003) respectively. The results for the same operating mode but assuming a settling velocity of 0.1 $mm.s^{-1}$ for the cohesive class are shown in Figure 3-30 and Figure 3-31.

The backhoe simulations assumed uniform sediment release across the water column (within a 32m radius around the considered site) to reproduce losses from the bucket as it moves up and down. As a result, the *ssc* levels are relatively similar across the three vertical levels considered. The largest *ssc* contours have circular shapes and the plume becomes elongated along a northeast-southwest axis i.e. aligned with the shipping channel further away from the releases.

Figure 3-27 Backhoe dredging – the backhoe is placed onto a barge and dispose removed sediment into the Pukunui vessel.

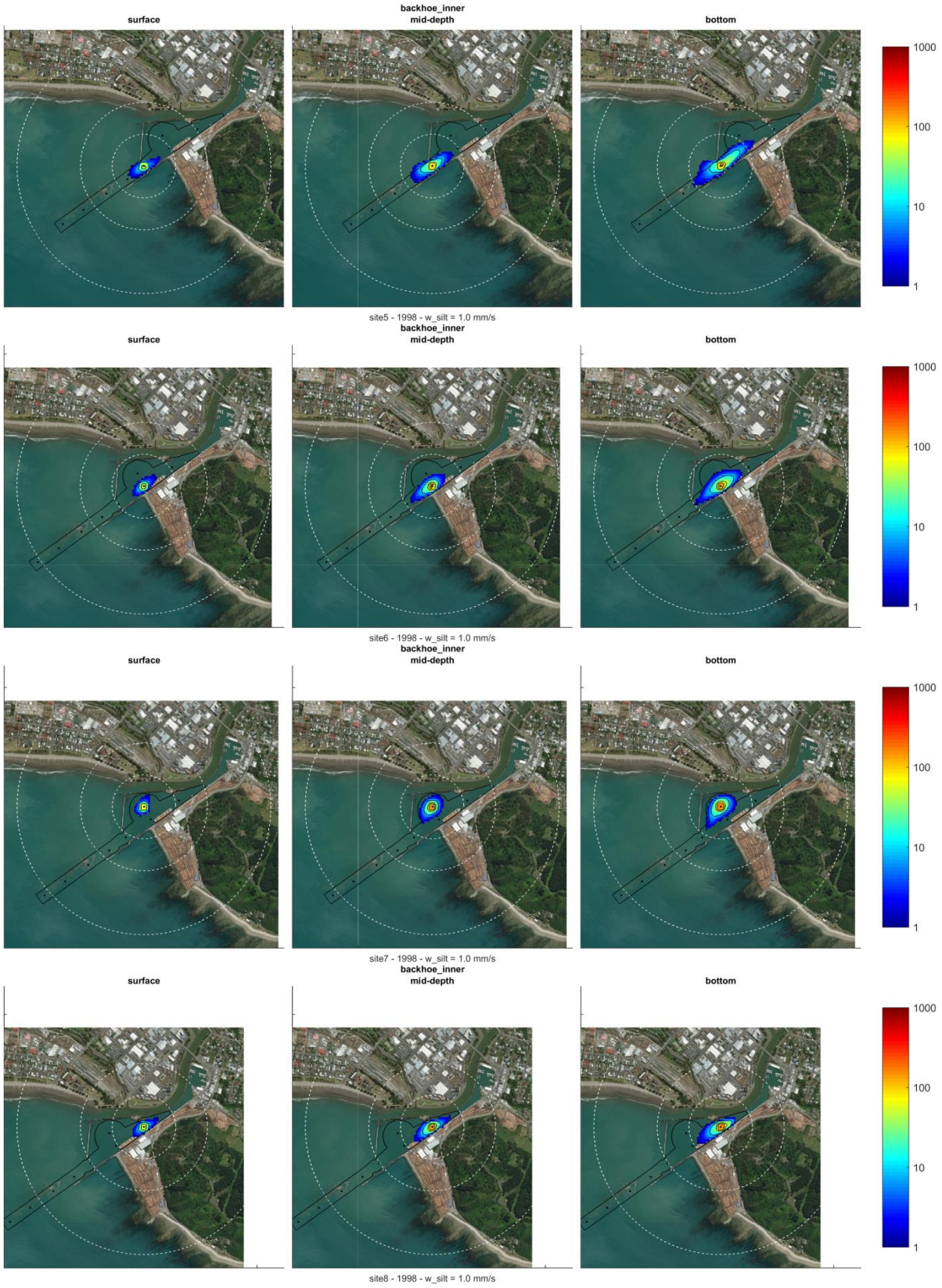

Figure 3-28 Probabilistic *ssc* fields [mg.L^{-1}] while dredging **with a backhoe**, in the inner channel (sites 5-8), derived from the annual La Niña period (June 1998-June 1999). The results assumed a settling velocity of 1 mm.s^{-1} for the cohesive sediment class. Dashed white circles have radiuses of 250, 500 and 1000 m. The 10, 50 and 100 mg.L^{-1} contours are shown in black.

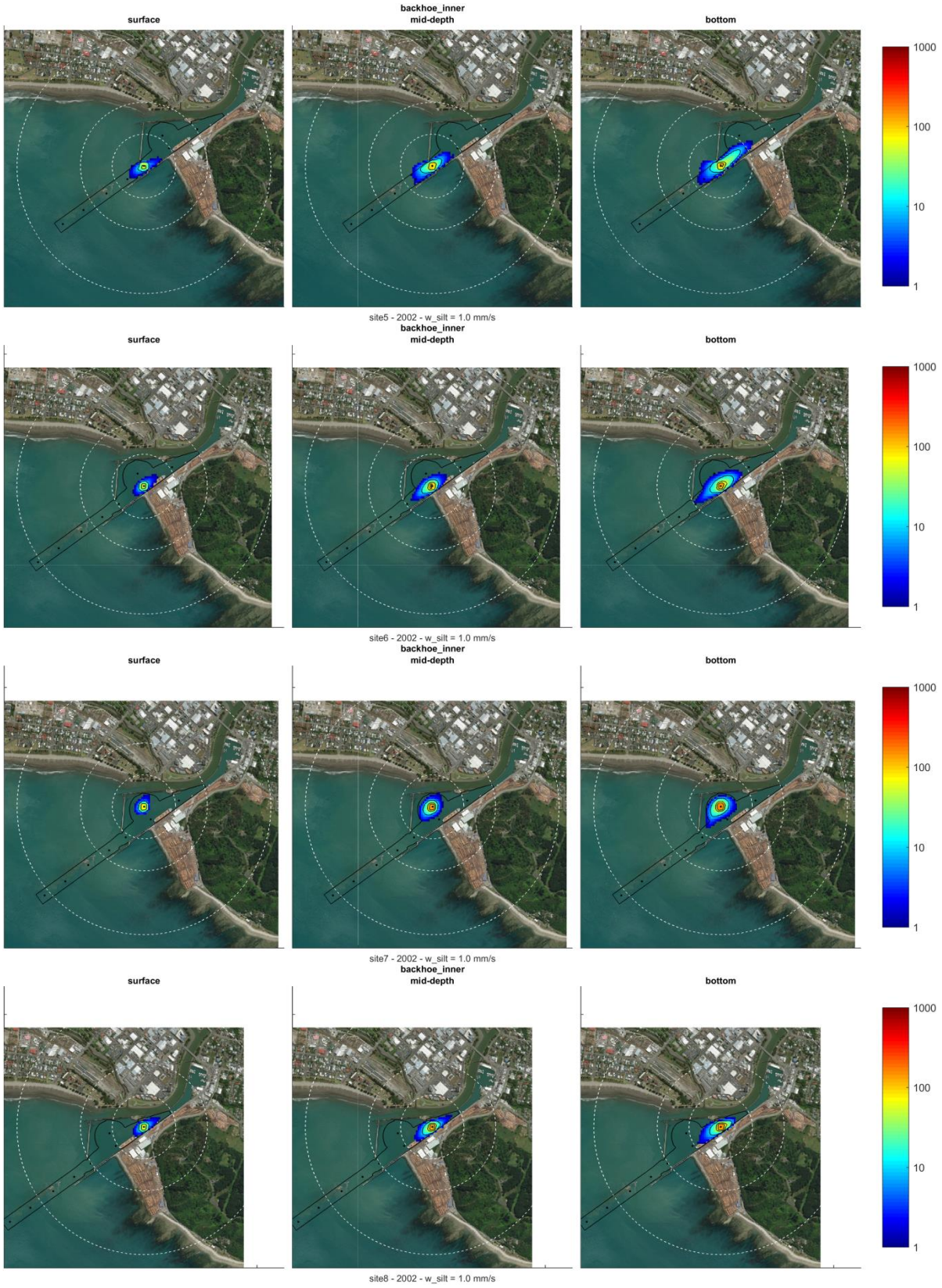

Figure 3-29 Probabilistic *ssc* fields [mg.L^{-1}] while dredging **with a backhoe**, in the inner channel (sites 5-8), derived from the annual El Niño period (June 2002-June 2003). The results assumed a settling velocity of 1 mm.s^{-1} for the cohesive sediment class. Dashed white circles have radiuses of 250, 500 and 1000 m. The 10, 50 and 100 mg.L^{-1} contours are shown in black.

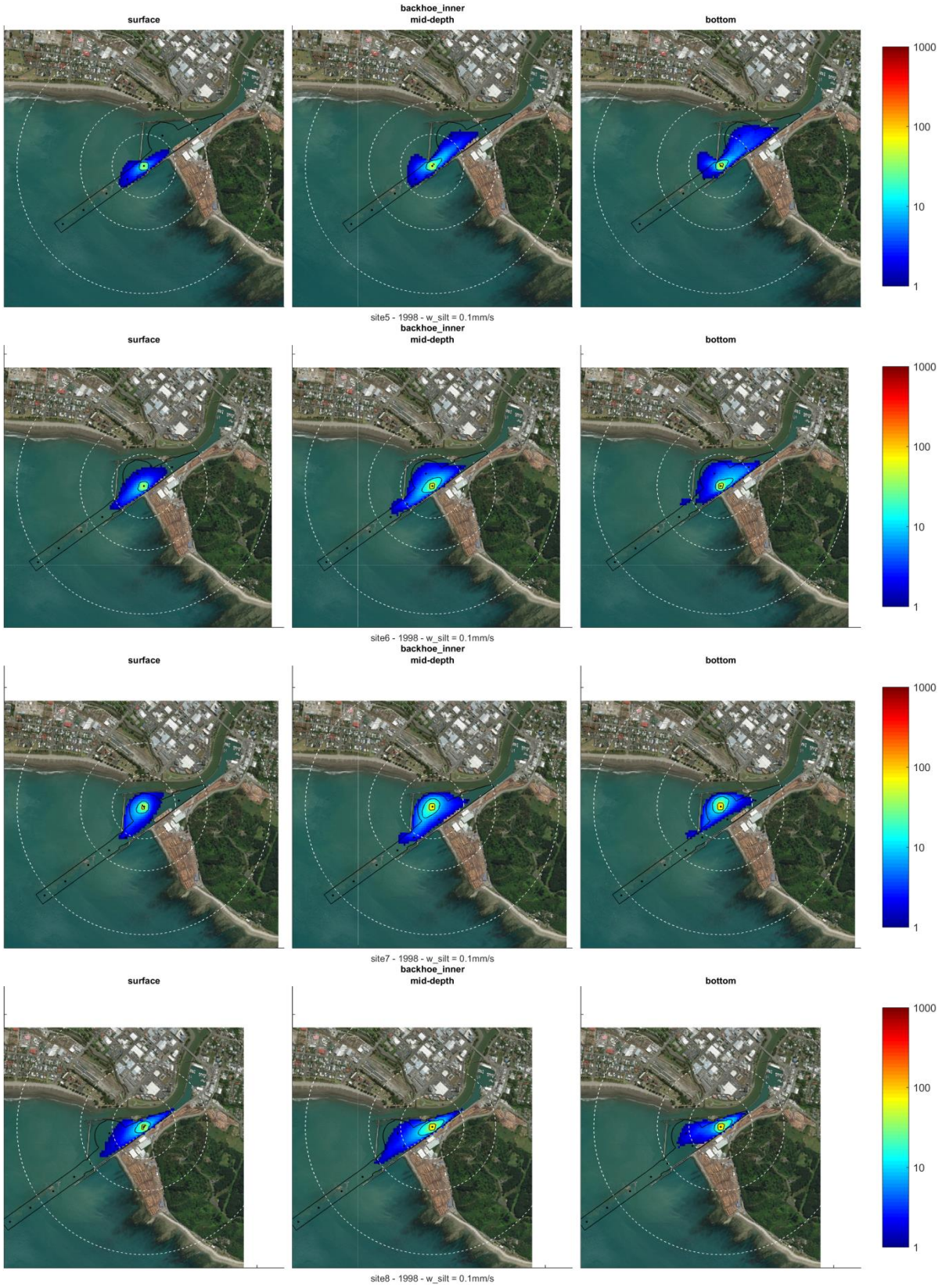

Figure 3-30 Probabilistic *ssc* fields [mg.L^{-1}] while dredging **with a backhoe**, in the inner channel (sites 5-8), derived from the annual La Niña period (June 1998-June 1999). The results assumed a settling velocity of 0.1 mm.s^{-1} for the cohesive sediment class. Dashed white circles have radiuses of 250, 500 and 1000 m. The 10, 50 and 100 mg.L^{-1} contours are shown in black.

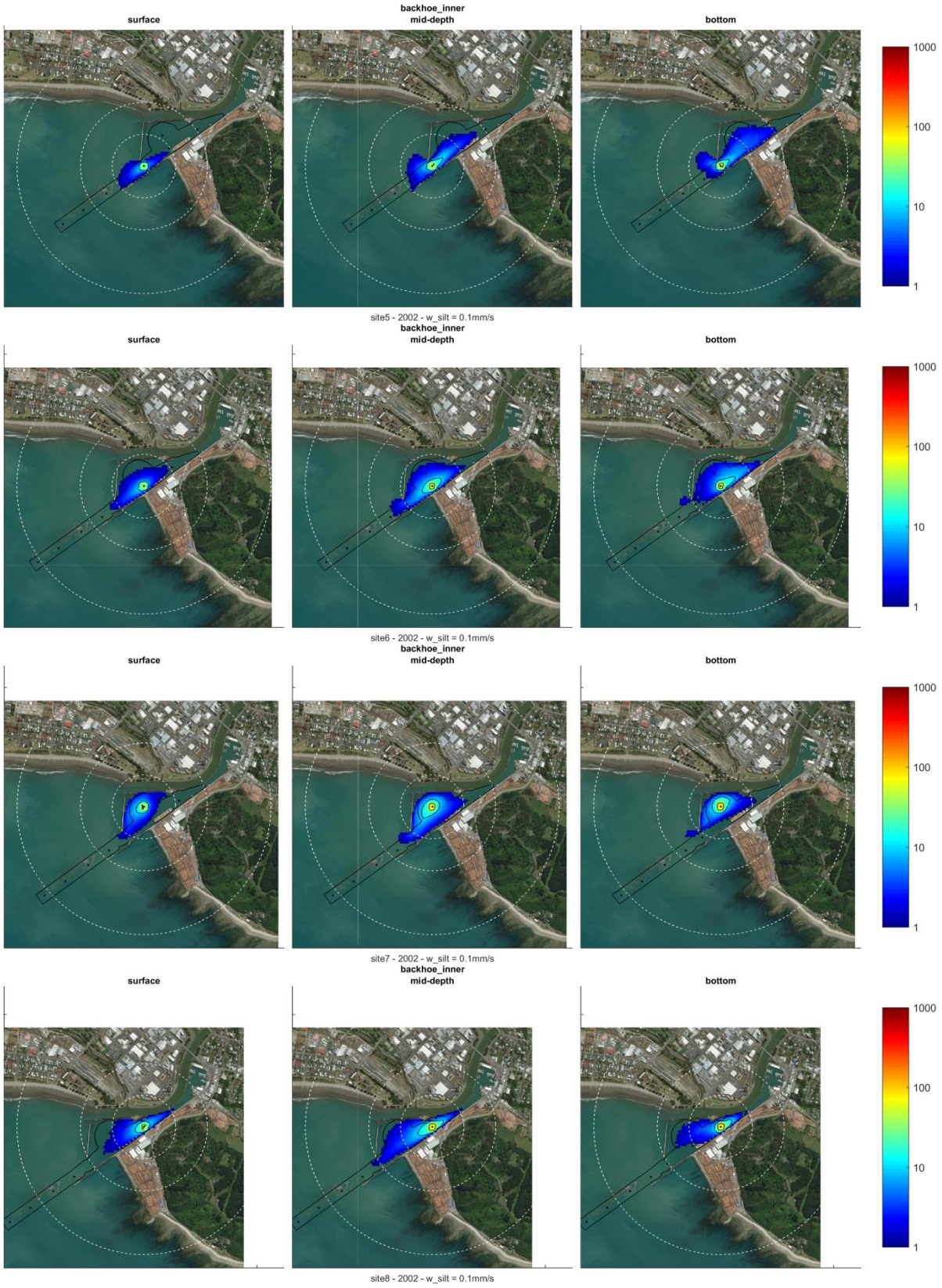

Figure 3-31 Probabilistic *ssc* fields [mg.L^{-1}] while dredging **with a backhoe**, in the inner channel (sites 5-8), derived from the annual El Niño period (June 2002-June 2003). The results assumed a settling velocity of 0.1 mm.s^{-1} for the cohesive sediment class. Dashed white circles have radiuses of 250, 500 and 1000 m. The 10, 50 and 100 mg.L^{-1} contours are shown in black.

4. SUMMARY

The objective of the present report was to characterise the dispersion patterns of the sediment plumes produced during the dredging of the shipping channel.

Dredging sediment plume dispersal was simulated using particle-tracking simulations during two different 1-year periods with contrasting historical climate contexts, namely El Niño/La Niña episodes. The dredging operations are simulated in the particle-tracking model through the use of different sediment source terms representing processes by which sediment is suspended into the water column during the dredging and overflow phases. The released sediment becomes subject to advection and diffusion by the ambient current forcing, forming a passive plume.

Two different dredging methods were considered, namely dredging using the Trailer Suction Hopper dredger Pukunui (480 m^3 hopper) that is currently used for maintenance dredging and dredging using backhoe (for areas not reachable by Pukunui). Considered source terms included in the simulations include drag head disturbance, propeller wash, de-entrainment from released overflow mixture, nearbed density current, surface losses, and bucket losses for backhoe dredging.

Given the uncertainties associated with the effective timing of the operations, as well as the *in-situ* characteristics of the dredged sediment, a probabilistic approach was followed whereby the long-term annual simulations are post-processed to provide robust statistical metrics of the *ssc* plume dispersions. Two different sediment settling velocities were considered for the cohesive fraction to account for uncertainties on the flocculation effects. These probabilistic *ssc* plume footprints and magnitudes provide useful metrics for impact assessments and comparison of dredging techniques.

The general plume dispersion patterns vary along the shipping channel following ambient current regimes. Dispersion pattern are typically elliptical, with an elongation northwest-southeast, along the outer channel; this component is conserved moving towards the Port entrance, but becomes combined with an increasing northeast-southwest dispersion feature associated with the “flushing” flows in and out Port basin, constrained by the narrow Port entrance. Dispersion patterns further into the Port basin become elongated in the northeast-southwest direction, following the general channel orientation.

5. REFERENCES

Beamsley, B.J., 2003. Nearshore sediment dynamics in a mixed sand/mud environment (D Phil Earth Sciences). University of Waikato, Hamilton, N.Z.

Becker J., van Eekelen E., van Wiechen J., de Lange W., Damsma T., Smolders T., van Koningsveld M., 2015. Estimating source terms for far field dredge plume modelling. J. Environ. Manage. 149, 282–293.

Bellasio, R., Bianconi,R, Mosca, S., Zannetti, P., 2017. Formulation of the Lagrangian particle model LAPMOD and its evaluation against Kincaid SF6 and SO2 datasets. Atmos. Environ. 163, 87–98.

Botev, Z. I, Grotowski, J. F, Kroese, D.P, 2010. Kernel density estimation via diffusion. Ann. Stat. 38, 2916–2957.

De Haan, P., 1999. On the use of density kernels for concentration estimations within particle and puff dispersion models. Atmos. Environ. 33, 2007–2021.

Elder, J.W., 1956. The dispersion of marked fluid in turbulent shear flow. J. Fluid Mech. 5, 544–560.

Fischer, H.B., Koh, R.C.Y., Imberger, J., Brooks, N.H., 1979. Mixing in Inland and Coastal Waters. Academic Press, San Diego, Califonia USA.

MetOcean Solutions, 2018. Eastland Port Maintenance Dredging and Disposal Project. Disposal plume modelling (No. P0331- 07).

MetOcean Solutions, 2017. Eastland Port Maintenance Dredging and Disposal Project. Hydrodynamic hindcast validation (No. P0331- 01).

Okubo, A., 1971. Oceanic diffusion diagrams. Deep-Sea Res. 18, 789–802.

Silverman, B.W, 1986. Density Estimation for Statistics and Data Analysis, Chapman and Hall Ltd. ed. London.

Smith, S.J., Friedrichs, C.T., 2011. Size and settling velocities of cohesive flocs and suspended sediment aggregates in a trailing suction hopper dredge plume. Cont. Shelf Res., Proceedings of the 9th International Conference on Nearshore and Estuarine Cohesive Sediment Transport Processes 31, S50–S63. https://doi.org/10.1016/j.csr.2010.04.002

Spearman, J., Bray, R.N., Land, J., Burt, T.N., Mead, C.T., Scott, D., 2007. Plume dispersion modelling using dynamic representation of trailer dredger source terms, in: J.P.-Y. Maa, L.P.S. and D.H.S. (Ed.), Proceedings in Marine Science, Estuarine and Coastal Fine Sediments DynamicsIntercoh 2003. Elsevier, pp. 417–448.

Van Rijn, L.C., 2007. A unified view of sediment transport by current and waves, Part II. J. Hydraul. Eng. ASCE.

Vitali, L., Monforti, F., Bellasio, R., Bianconi, R., Sachero, V., Mosca, S., Zanini, G., 2006. Validation of a Lagrangian dispersion model implementing different kernel methods for density reconstruction. Atmos. Environ. 40, 8020–8033.

Whitehouse R., Soulsby R., Robert W., Mitchener H., 2000. Dynamics of estuarine muds, Thomas Telford, London. ed.

Winterwerp, J.C., 2002. Near-field behavior of dredging spill in shallow water. J. Waterw. Port Coast. Ocean Eng. 128, 96–98.

Zhang, Y.J., Ateljevich, E., Yu, H.-C., Wu, C.H., Jason, C.S., 2015. A new vertical coordinate system for a 3D unstructured-grid model. Ocean Model. 85, 16–31.

Zhang, Y.L., Baptista, A.M., 2008. A semi-implicit Eulerian-Lagrangian finite element model for cross-scale ocean circulation. Ocean Model. 21, 71–96.

6. APPENDIX A

Table 6.1 Sources terms for the Pukunui vessel dredging at the outer sites 1-4 (sediment 80% sand, 20% cohesive).

Vessel and Cycle	**Units**	**Variables names (Becker et al., 2015)**	
Capacity [$mm.s^{-1}$]			480
Dredging cycle			
Hopper infilling - total time	**[hours]**	**t2-t0**	2
Including infilling with no overflow	**[hours]**	**t1-t0**	0.5
Including overflow time	**[hours]**	**t2-t1**	1.5
Overflow loading ratio	**[-]**	**(t2-t1)/(t2-t0)**	0.75
Travel to and from disposal site	**[hours]**	**t3-t2**	2
Disposal time	**[hours]**	**t4-t3**	-
Production Rate			
Dry density	**[kg.m-3]**		1350
Amount of sediment removed per cycle	**[m3]**	**Vt**	220
Amount of sediment removed per cycle	**[kg]**	**Mt**	297,000
Production Rate	**[m3.s-1]**	**Vt/ (t2-t0)**	0.030555556
Production Rate	**[kg.s-1]**	**Mt/ (t2-t0)**	41.25
Source terms - masses			
Propeller wash(1.5%)	**[kg]**	**m_prop**	4,455
Drag head (1.5%)	**[kg]**	**m_drag**	4,455
Surface losses (1%)	**[kg]**	**m_surface**	2,970
Remaining mass transported in hopper	**[kg]**	**Mh = Mt - m_prop -m_drag - m_surface**	285,120
Mass exiting through overflow	**[kg]**	**Mo =[[(t2-t1)/(t2-t0)]*(1-fsett)*(1-ftrap)] * Mh**	152,361
Diffuse overflow (20%)	**[kg]**	**m_overflow_diffuse**	30,472
Mass remaining in hopper at end of cycle	**[kg]**	**M_remaining = Mh - Mo**	132,759
Source terms - mass fluxes			
Propeller wash(1.5%)	**[kg.s-1]**	**m_prop/(t2-t0)**	0.62
Drag head (1.5%)	**[kg.s-1]**	**m_drag/(t2-t0)**	0.62
Surface losses (1%)	**[kg.s-1]**	**m_surface/(t2-t0)**	0.41
Diffuse overflow (20%)	**[kg.s-1]**	**m_overflow_diffuse/(t2-t1)**	5.64
Disposal	**[kg.s-1]**	**M_remaining /(t4-t3)**	-

Table 6.2 Sources terms for the Pukunui vessel dredging at the inner sites 5-8 (sediment 80% cohesive, 20% sand).

Vessel and Cycle	Units	Variables names (Becker et al., 2015)	
Capacity [$mm.s^{-1}$]			480
Dredging cycle			
Hopper infilling - total time	**[hours]**	**t2-t0**	2
Including infilling with no overflow	**[hours]**	**t1-t0**	0.5
Including overflow time	**[hours]**	**t2-t1**	1.5
Overflow loading ratio	**[-]**	**(t2-t1)/(t2-t0)**	0.75
Travel to and from disposal site	**[hours]**	**t3-t2**	2
Disposal time	**[hours]**	**t4-t3**	-
Production Rate			
Dry density	**[kg.m-3]**		650
Amount of sediment removed per cycle	**[m3]**	**Vt**	220
Amount of sediment removed per cycle	**[kg]**	**Mt**	143,000
Production Rate	**[m3.s-1]**	**Vt/ (t2-t0)**	0.030555556
Production Rate	**[kg.s-1]**	**Mt/ (t2-t0)**	19.86111111
Source terms - masses			
Propeller wash(1.5%)	**[kg]**	**m_prop**	2,145
Drag head (1.5%)	**[kg]**	**m_drag**	2,145
Surface losses (1%)	**[kg]**	**m_surface**	1,430
Remaining mass transported in hopper	**[kg]**	**Mh = Mt - m_prop -m_drag - m_surface**	137,280
Mass exiting through overflow	**[kg]**	**Mo =[[(t2-t1)/(t2-t0)]*(1-fsett)*(1-ftrap)] * Mh**	73,359
Diffuse overflow (20%)	**[kg]**	**m_overflow_diffuse**	14,672
Mass remaining in hopper at end of cycle	**[kg]**	**M_remaining = Mh - Mo**	63,921
Source terms - mass fluxes			
Propeller wash(1.5%)	**[kg.s-1]**	**m_prop/(t2-t0)**	0.30
Drag head (1.5%)	**[kg.s-1]**	**m_drag/(t2-t0)**	0.30
Surface losses (1%)	**[kg.s-1]**	**m_surface/(t2-t0)**	0.20
Diffuse overflow (20%)	**[kg.s-1]**	**m_overflow_diffuse/(t2-t1)**	2.72
Disposal	**[kg.s-1]**	**M_remaining /(t4-t3)**	-

Table 6.3 Sources terms for the backhoe dredging at the inner sites 5-8 (sediment 80% cohesive, 20% sand).

Vessel and Cycle	**Units**	**Variables names (Becker et al., 2015)**	
Capacity [$mm.s^{-1}$]			480
Dredging cycle			
Hopper infilling - total time	**[hours]**	**t2-t0**	4
Travel to and from disposal site	**[hours]**	**t3-t2**	2
Disposal time	**[hours]**	**t4-t3**	-
Production Rate			
Dry density	**[kg.m-3]**		650
Amount of sediment removed per cycle	**[m3]**	**Vt**	220
Amount of sediment removed per cycle	**[kg]**	**Mt**	143,000
Production Rate	**[m3.s-1]**	**Vt/ (t2-t0)**	0.015277778
Production Rate	**[kg.s-1]**	**Mt/ (t2-t0)**	9.930555556
Source terms - masses			
Backhoe source term (4%)	**[kg]**	**m_backhoe**	5,720
Source terms - mass fluxes			
Backhoe source term (4%)	**[kg.s-1]**	**m_backhoe/(t2-t0)**	0.40
Disposal	**[kg.s-1]**	**M_remaining /(t4-t3)**	-